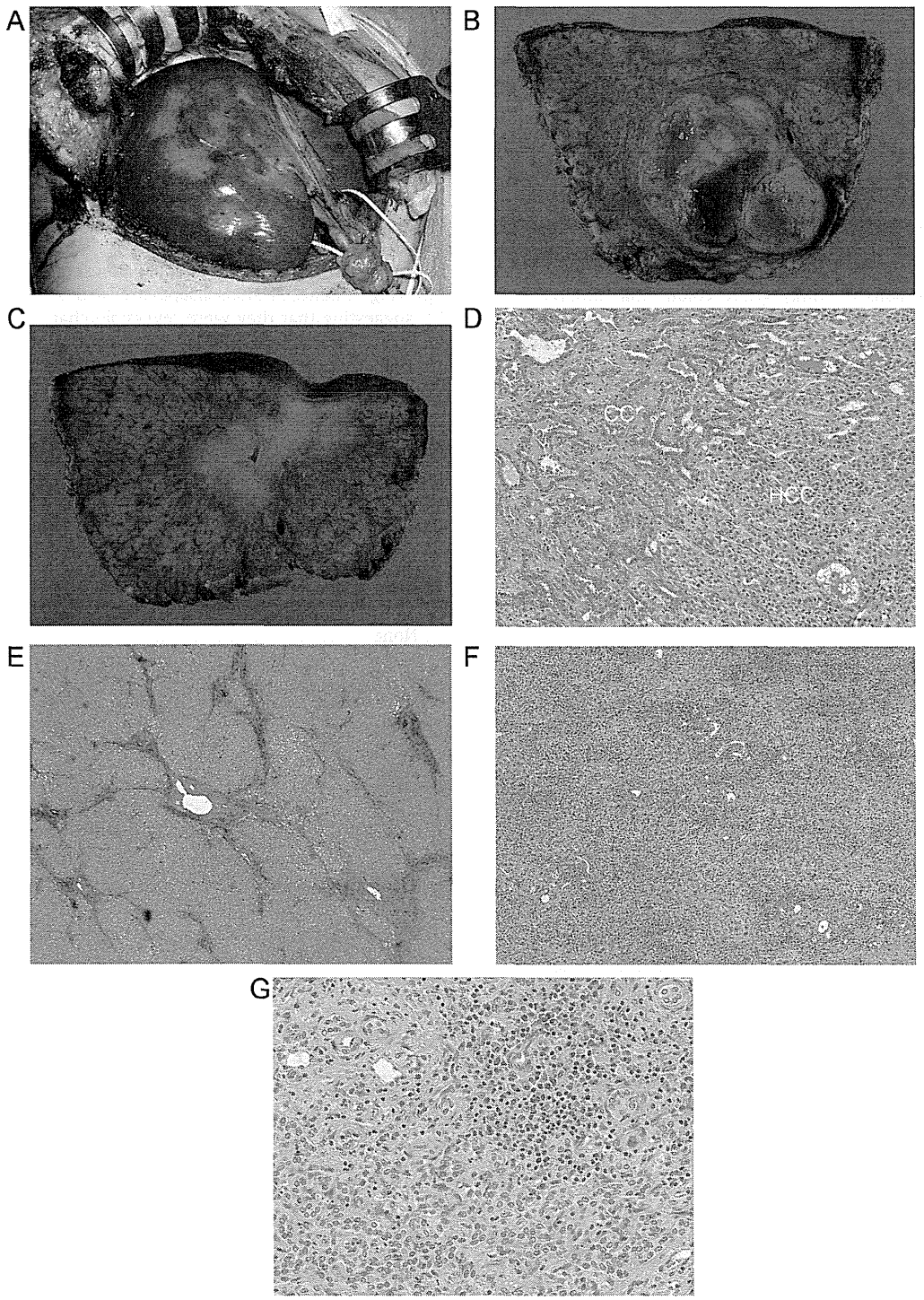

Fig. 4. During the surgery, several white pitted scars were observed on the surface of the liver (Panel A). Gross photograph of resected specimen showed a yellowish-white tumour with capsule (Panel B). Milky white lesions existed in the specimen separated from the tumour (Panel C). The photomicrograph of the cHCC-CC nodule showed both increased cell density with trabecular pattern and pseudoglandular pattern (Panel D, HCC: hepatocellular carcinoma) and irregular glandular structure (Panel D, CC: cholangiocarcinoma). Nonneoplastic lesions showed loss of hepatocytes, lymphoplasmacytic infiltration, proliferation of bile ductules, and mild fibrosis (Panel F and G). The background liver showed chronic hepatitis, F3/A1 in METAVIR system (E).

accompanied by depression, whereas others in inward liver were nodular (Fig. 2A and C). Gadolinium-ethoxybenzyl-diethylenetriamine pentaacetic acid (Gd-EOB-DTPA)-enhanced magnetic resonance imaging (MRI) revealed a distinct defect in the hepatobiliary phase in the nodule suspected of being HCC and an indistinct defect in others (Fig. 3). The enhancement pattern in the arterial phase of each lesion was similar to that in contrast-enhanced CT. Ultrasonography-guided biopsy was performed from the former nodule in segment 5 (Fig. 1A) and a lesion in segment 6 (Fig. 1C). Histological evaluation indicated the nodule in segment

5 to be cHCC-CC. No neoplastic cell was found in the lesion in segment 6.

We considered hyperbilirubinaemia to be due to drug-induced liver injury and changed the anti-HIV regimen, stopping atazanavir and ritonavir and adding raltegravir. Hyperbilirubinaemia was ameliorated thereafter. The patient underwent partial hepatic resection for cHCC-CC. During the surgery, several white pitted scars were observed on the surface of the liver (Fig. 4A). Diagnosis of cHCC-CC of classical type, the HCC component being immunoreactive for Hepatocyte antigen and the CC component for CK7 and CK19, was confirmed by pathological evaluation of the surgical specimen (Fig. 4B and D). In the specimen, there were several lesions of milky white colour that differed from the main tumour, corresponding to the multiple lesions on ultrasonography and CT (Fig. 4C). Pathologically, these lesions showed regional loss of hepatocytes, lymphoplasmacytic infiltration, proliferation of bile ductules and mild fibrosis (Fig. 4F and G). These lesions were localised panlobular necrosis and considered as a non-neoplastic, inflammatory process. Special stains (Gram, Ziehl–Neelsen, Periodic acid-Schiff (PAS) and Grocott) did not reveal any infectious agents, including bacteria, fungus or protozoa (*Toxoplasma*). Immunohistochemical staining for cytomegalovirus and *in situ* hybridisation for EBER were negative. The background liver showed chronic hepatitis, corresponding to F3/A1 in the METAVIR system[4,5] (Fig. 4E).

The patient is currently alive without recurrence for 2 years and the multiple ring-enhanced lesions have been undetectable in postoperative follow-up CT examinations.

3. Other similar and contrasting cases in the literature

This was a case with cHCC-CC accompanied by multiple hypervascular non-neoplastic lesions developed in a patient with HIV and HCV coinfection. In North America, Europe and Japan, HCV infection is the main risk factor for HCC.[6] Several studies also suggested that HCV infection was one of the risk factors for intrahepatic cholangiocarcinoma.[7,8] cHCC-CC is a rare form of primary liver cancer showing histopathological features of both HCC and cholangiocarcinoma.[9,10] As with the present case, cases of cHCC-CC arising from the liver of patients with HCV infection were previously reported in several studies.[11–14] Furthermore, Shaib et al. reported that HIV was one of the risk factors of intrahepatic cholangiocarcinoma along with HCV.[8] Not only HCV but also HIV infection may have played a role in carcinogenesis in this case. There are no other reports of cHCC-CC development in HIV and HCV coinfected patients. There are also no other reports of multiple non-neoplastic hypervascular lesions in the liver of patients undergoing HIV treatment as this case.

4. Discussion

The present case was coinfected with HIV and HCV. Previous studies demonstrated that HIV infection accelerates HCV-related liver-fibrosis progression, and the lower CD4 count is associated with the higher rate of liver-fibrosis progression.[15–17] It was also reported that HCC develops at a younger age and after a shorter period of HCV infection in HIV and HCV coinfected patients than in HCV-monoinfected patients.[18,19] Considering the fact that the present case developed HCC at a younger age than typical HCV-related HCC patients with CD4 count <200 cells μl^{-1}, HIV infection was likely to have accelerated liver fibrosis and carcinogenesis.

This case was also quite interesting in that cHCC-CC and multiple non-neoplastic lesions with impressive radiological findings coexisted in the liver. If based solely on radiologic findings, differential diagnosis would include HCC, cholangiocarcinoma, metastatic liver cancer, malignant lymphoma, epithelioid haemangioendothelioma, hepatic peliosis, Kaposi's sarcoma and inflammatory pseudotumour. Needle biopsy revealed that solitary cHCC-CC and multiple non-neoplastic lesions coexisted. Pathological investigation after surgery suggested that these non-neoplastic lesions were post-inflammatory changes representing residues of panlobular necrosis. Although we suspected fulminant or subacute viral hepatitis or autoimmune hepatitis as a cause of panlobular necrosis, we could not find clinical information that would confirm such diagnosis. We also suspected drug-induced liver injury caused by HAART as a cause of panlobular necrosis. However, there were no other reports of such lesions in the liver of patients receiving HAART. Multiple ring-enhanced lesions disappeared in postoperative follow-up CT, suggesting that they were reversible changes. It may be possible that the multiple non-neoplastic lesions were pathological changes associated with immune disorder caused by HIV infection, immune reconstruction inflammatory syndrome caused by HAART, antiretroviral drug-induced liver injury or infection which we could not diagnose.

Funding

None.

Competing interests

None.

Ethical approval

Not required.

Disclosure

The authors have nothing to disclose.

Acknowledgements

This work was supported in part by Health Sciences Research Grants of The Ministry of Health, Labour and Welfare of Japan (Research on Hepatitis).

References

1. Koziel MJ, Peters MG. Viral hepatitis in HIV infection. *N Engl J Med* 2007;**356**:1445–54.
2. Koike K, Tsukada K, Yotsuyanagi H, Moriya K, Kikuchi Y, Oka S, et al. Prevalence of coinfection with human immunodeficiency virus and hepatitis C virus in Japan. *Hepatol Res* 2007;**37**:2–5.
3. Joshi D, O'Grady J, Dieterich D, Gazzard B, Agarwal K. Increasing burden of liver disease in patients with HIV infection. *Lancet* 2011;**377**:1198–209.
4. The French METAVIR Cooperative Study Group. Intraobserver and interobserver variations in liver biopsy interpretation in patients with chronic hepatitis C. *Hepatology* 1994;**20**:15–20.
5. Bedossa P, Poynard T, The METAVIR Cooperative Study Group. An algorithm for the grading of activity in chronic hepatitis C. *Hepatology* 1996;**24**:289–93.
6. Forner A, Llovet JM, Bruix J. Hepatocellular carcinoma. *Lancet* 2012;**379**:1245–55.
7. Shaib Y, El-Serag HB. The epidemiology of cholangiocarcinoma. *Semin Liver Dis* 2004;**24**:115–25.
8. Shaib YH, El-Serag HB, Davila JA, Morgan R, McGlynn KA. Risk factors of intrahepatic cholangiocarcinoma in the United States: a case–control study. *Gastroenterology* 2005;**128**:620–6.
9. Allen RA, Lisa JR. Combined liver cell and bile duct carcinoma. *Am J Pathol* 1949;**25**:647–55.
10. Goodman ZD, Ishak KG, Langloss JM, Sesterhenn IA, Rabin L. Combined hepatocellular-cholangiocarcinoma. A histologic and immunohistochemical study. *Cancer* 1985;**55**:124–35.
11. Taguchi J, Nakashima O, Tanaka M, Hisaka T, Takazawa T, Kojiro M. A clinicopathological study on combined hepatocellular and cholangiocarcinoma. *J Gastroenterol Hepatol* 1996;**11**:758–64.

12. Jarnagin WR, Weber S, Tickoo SK, Koea JB, Obiekwe S, Fong Y, et al. Combined hepatocellular and cholangiocarcinoma: demographic, clinical, and prognostic factors. *Cancer* 2002;**94**:2040–6.
13. Yano Y, Yamamoto J, Kosuge T, Sakamoto Y, Yamasaki S, Shimada K, et al. Combined hepatocellular and cholangiocarcinoma: a clinicopathologic study of 26 resected cases. *Jpn J Clin Oncol* 2003;**33**:283–7.
14. Cazals-Hatem D, Rebouissou S, Bioulac-Sage P, Bluteau O, Blanche H, Franco D, et al. Clinical and molecular analysis of combined hepatocellular-cholangiocarcinomas. *J Hepatol* 2004;**41**:292–8.
15. Benhamou Y, Bochet M, Di Martino V, Charlotte F, Azria F, Coutellier A, et al. Liver fibrosis progression in human immunodeficiency virus and hepatitis C virus coinfected patients. *Hepatology* 1999;**30**:1054–8.
16. Mohsen AH, Easterbrook PJ, Taylor C, Portmann B, Kulasegaram R, Murad S, et al. Impact of human immunodeficiency virus (HIV) infection on the progression of liver fibrosis in hepatitis C virus infected patients. *Gut* 2003;**52**:1035–40.
17. Yotsuyanagi H, Kikuchi Y, Tsukada K, Nishida K, Kato M, Sakai H, et al. Chronic hepatitis C in patients co-infected with human immunodeficiency virus in Japan: a retrospective multicenter analysis. *Hepatol Res* 2009;**39**:657–63.
18. Garcia-Samaniego J, Rodriguez M, Berenguer J, Rodriguez-Rosado R, Carbo J, Asensi V, et al. Hepatocellular carcinoma in HIV-infected patients with chronic hepatitis C. *Am J Gastroenterol* 2001;**96**:179–83.
19. Brau N, Fox RK, Xiao P, Marks K, Naqvi Z, Taylor LE, et al. Presentation and outcome of hepatocellular carcinoma in HIV-infected patients: a U.S. -Canadian multicenter study. *J Hepatol* 2007;**47**:527–37.

SCIENTIFIC REPORTS

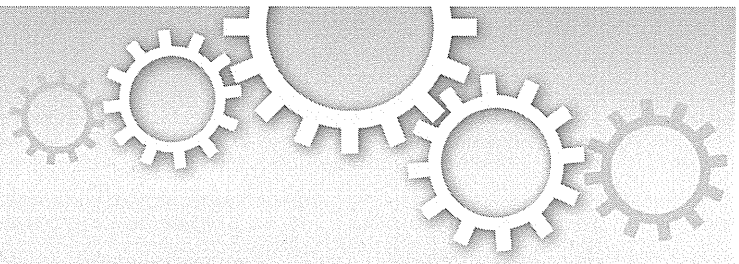

OPEN

SUBJECT AREAS:
MIRNAS
NUTRIENT SIGNALLING
NATURAL PRODUCTS
TYPE 2 DIABETES MELLITUS

Received
10 May 2013

Accepted
15 August 2013

Published
30 August 2013

Correspondence and requests for materials should be addressed to M.O. (otsukamo-tky@umin.ac.jp)

* These authors contributed equally to this work.

The flavonoid apigenin improves glucose tolerance through inhibition of microRNA maturation in miRNA103 transgenic mice

Motoko Ohno[1]*, Chikako Shibata[1]*, Takahiro Kishikawa[1], Takeshi Yoshikawa[1], Akemi Takata[1], Kentaro Kojima[1], Masao Akanuma[2], Young Jun Kang[3], Haruhiko Yoshida[1], Motoyuki Otsuka[1,4] & Kazuhiko Koike[1]

[1]Department of Gastroenterology, Graduate School of Medicine, The University of Tokyo, Tokyo 113-8655, Japan, [2]Division of Gastroenterology, The Institute for Adult Diseases, Asahi Life Foundation, Tokyo 100-0005, Japan, [3]Department of Immunology and Microbial Sciences, The Scripps Research Institute, La Jolla, CA 92037, USA, [4]Japan Science and Technology Agency, PRESTO, Kawaguchi, Saitama 332-0012, Japan.

Polyphenols are representative bioactive substances with diverse biological effects. Here, we show that apigenin, a flavonoid, has suppressive effects on microRNA (miRNA) function. The effects were mediated by impaired maturation of a subset of miRNAs, probably through inhibition of the phosphorylation of TRBP, a component of miRNA-generating complexes via impaired mitogen-activated protein kinase (MAPK) Erk activation. While glucose intolerance was observed in miRNA103 (miR103)-overexpressing transgenic mice, administration of apigenin improved this pathogenic status likely through suppression of matured miR103 expression levels. These results suggest that apigenin may have favorable effects on the pathogenic status induced by overexpression of miRNA103, whose maturation is mediated by phosphorylated TRBP.

Polyphenols, common components of many popular drinks and foods, and caffeine, an alkaloid in various seeds and leaves, are representative bioactive substances with diverse biological effects[1,2]. However, while some effects have been examined in detail[3], the molecular mechanisms underlining these biological effects are mostly undetermined.

MicroRNAs (miRNAs) are short, single-stranded, non-coding RNAs expressed in most organisms ranging from plants to vertebrates[4]. Primary miRNAs, which possess stem-loop structures, are processed into mature miRNAs by Drosha, Dicer, RNA polymerase III, and other related molecules. These mature miRNAs then bind the RNA-induced silencing complex (RISC), and the resulting co-complex directly binds the 3′-untranslated regions (3′-UTRs) of target mRNAs to act as suppressors of translation and gene expression. Thus, dependent upon the identity of the target mRNAs, miRNAs are responsible for the control of various biological functions, including cell proliferation, apoptosis, differentiation, metabolism, oncogenesis, and oncogenic suppression[5–9]. For example, it was reported recently that expression of miRNA103 and 107 (miR103 and 107) was upregulated in obese mice, and that the gain of miR103 function in either liver or fat was sufficient to induce impaired glucose homeostasis[10].

Because the effects of bioactive substances are diverse and the functions of miRNAs result in diverse biological consequences, we hypothesized that some effects of bioactive substances may depend on modulation of miRNA function. In this study, we examined whether polyphenols and caffeine affect miRNA function and determined the molecular mechanisms underlying these effects. In addition, we applied the results obtained here to clinically relevant models to facilitate their use in practical applications.

Results

Apigenin suppresses miRNA function. To determine the effects of polyphenols and caffeine on miRNA function, we determined the luciferase activities of several types of reporters constructed containing

miRNA-binding sites (the function of which is suppressed by corresponding miRNAs) upon treatment with caffeine or polyphenols. The polyphenols used here were apigenin, procyanidin A2 and procyanidin B2 from flavonoids, and chlorogenic acid from phenolic acid. A cell line derived from the liver, Huh7, was used because substances in food theoretically flow into the liver first through the portal vein immediately after intestinal absorption. Among the bioactive substances examined, only apigenin significantly inhibited the effects of miRNAs such as miR122, miR185 and miR103 (Figure 1a), which are highly expressed in the liver[11]. The effects were similarly observed irrespective of endogenous miRNAs or exogenous overexpression of corresponding miRNAs (Figure 1a and b) in a dose-dependent manner (Figure 1c). Another liver cell line, Hep3B, showed similar results, suggesting that the effects were not cell line-specific (Supplementary Figure 1a, b and c). The effects were detected with 5 μM apigenin; this concentration is physiologically attainable[12–14]. These results suggest that apigenin has suppressive effects on miRNA function.

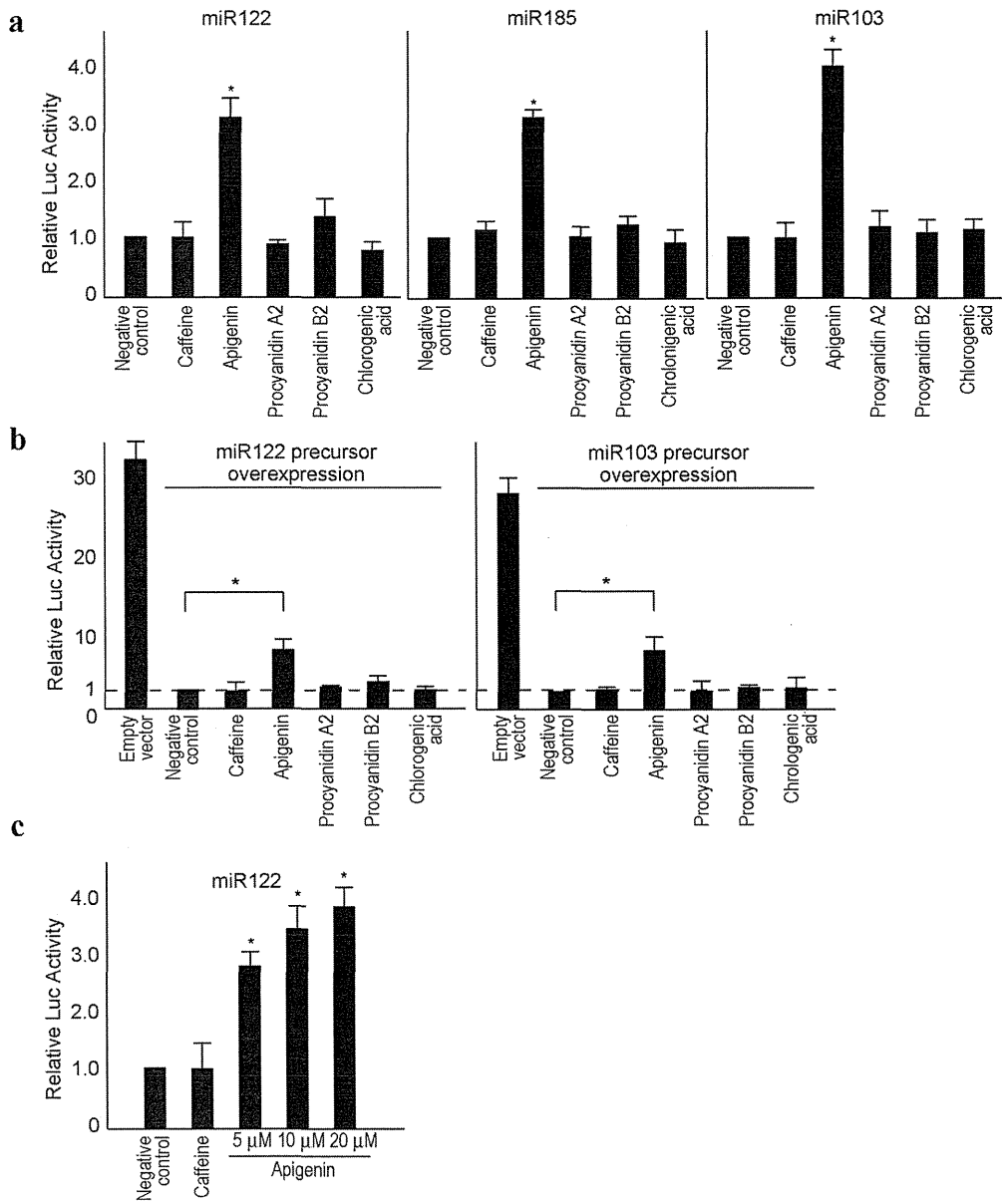

Figure 1 | Apigenin inhibits miRNA function. (a), Apigenin inhibits endogenous miRNA function. Huh7 cells were transfected with reporters to determine the functions of the indicated miRNAs. Twenty-four hours after treatment with the indicated substances, reporter assays were performed. Data represent the means ± standard deviation (s.d.) from three independent experiments. *, $p < 0.05$ (*t*-test). (b), Apigenin inhibits the function of exogenously overexpressed miRNAs. Huh7 cells were transfected with reporters and corresponding miRNA precursor-expressing plasmids or an empty vector. Twenty-four hours after treatment with the indicated substances, reporter assays were performed. Data represent the means ± s.d. from three independent experiments. *, $p < 0.05$ (*t*-test). (c), Dose-dependent effects of apigenin on miRNA function. Huh7 cells were transfected with reporter plasmids to determine miR122 function. Cells were treated with indicated doses of apigenin for 24 h and luciferase assays were performed. Caffeine was included as a negative control. Data represent the means ± s.d. from three independent experiments. *, $p < 0.05$ (*t*-test) compared with the negative control.

Apigenin inhibits miRNA maturation from miRNA precursors. To elucidate the molecular mechanisms underlying the inhibitory effects of apigenin on miRNA function, we first determined the expression levels of miRNA pathway-related molecules including Drosha, DGCR8, KSRP, Argonaute 2 (Ago2), and Dicer in the presence of apigenin. While the expression levels of Drosha, Ago2 and Dicer proteins appeared to decrease slightly after a high dose of apigenin, no significant changes were observed in the expression levels of these proteins (Figure 2a and Supplementary Figure 2a). Next, we examined the expression and maturation of miRNAs by quantitative real-time polymerase chain reaction (qRT-PCR) and Northern blotting (Figure 2b and Supplementary Figure 2b). Expression levels of mature endogenous miR122, miR103, and miR185 decreased and accumulation of precursor miRNAs was also observed after apigenin treatment (Figure 2b), suggesting that maturation from miRNA precursors was decreased. In addition, a comprehensive miRNA microarray analysis confirmed that apigenin altered the expression levels of a major subset of miRNAs (Supplementary Figure 2c; the raw data were deposited in the GEO database; GSE46526). However, some miRNAs, such as let-7, were not affected by apigenin treatment, which was confirmed by qRT-PCR (Figure 2b). These results suggest that apigenin has an inhibitory effect on the maturation of a subset of miRNAs.

Apigenin inhibits phosphorylation of TRBP. The microRNA-generating complex is composed of Dicer and phospho-TRBP isoforms[15], and TRBP phosphorylation enhances the maturation of a subset of miRNAs through stabilization of the microRNA-generating complexes[15]. Phosphorylation of TRBP is mediated by mitogen-activated protein kinase (MAPK) Erk[15]. Because apigenin is known to inhibit Erk activity[16–19], we hypothesized that the inhibitory effects of apigenin on miRNA maturation may be mediated by decreased phosphorylation of TRBP through inhibition of Erk. Consistent with previous reports, although caffeine had no effect on the Erk phosphorylation status, apigenin clearly inhibited Erk phosphorylation 24 h post-treatment without changes in total Erk levels (Figure 3a). Concordantly, SRE-driven reporter activities were diminished by apigenin treatment (Figure 3b), suggesting that apigenin indeed inhibited an Erk-mediated intracellular signaling pathway, consistent with previous reports[16–19]. While TRBP was phosphorylated under normal serum culture conditions, and its phosphorylation status did not change with caffeine treatment, its phosphorylation was inhibited by apigenin (Figure 3c). This effect was confirmed by electrophoresis in a phos-tag gel, which showed a clear slow-migrating band, indicating that TRBP was phosphorylated in control and caffeine-treated conditions, but its phosphorylation was inhibited upon treatment with apigenin (Figure 3d). To confirm that Erk activity was inhibited by apigenin following TRBP phosphorylation, we examined the effects of apigenin using Huh7 cells stably expressing constitutively active Mek1 (CA-MEK) on TRBP phosphorylation. As shown in Figure 3e, the degree of TRBP phosphorylation was increased only by CA-MEK expression, and the augmented phosphorylation was not diminished by apigenin treatment (Figure 3e), suggesting that the effects of apigenin could not be observed under the induced Erk activation. That is, the effects of apigenin were most probably mediated by inhibition of Erk activation. In addition, we established Huh7 cells stably expressing dominant negative Erk (DN-Erk). As predicted, the levels of mature miRNA103, 122, and 185, were decreased in DN-Erk expressing cells, but were slightly increased in CA-MEK expressing cells, irrespective of apigenin treatment (Figure 3f). The expression levels of mature let-7, which were examined as a representative miRNA that was not affected by apigenin treatment in the miRNA microarray (Figure 3f), were not changed by enforced expression of DN-Erk or CA-MEK, suggesting that this miRNA maturation is not significantly regulated by MAPK activity or TRBP phosphorylation, consistent with a previous report[15]. These results suggest that apigenin inhibits Erk phosphorylation, and subsequent decreased MAPK activity leads to a decrease in TRBP phosphorylation, which may result in decreased maturation of a subset of miRNAs.

Apigenin improves glucose tolerance through inhibition of miRNA function. To apply the above results in a clinical setting, we focused on recent findings demonstrating that a gain of miR103/107 expression induces impaired glucose homeostasis *in vivo*[10]. To utilize this, we generated transgenic mice expressing a miR103 precursor under control of the CMV promoter (Supplementary Figure 3a). Overexpression of miR103 in these mice was confirmed by Northern blotting against mature miR103 in liver tissues (Figure 4a and Supplementary Figure 3b). No significant over-saturation of RISC

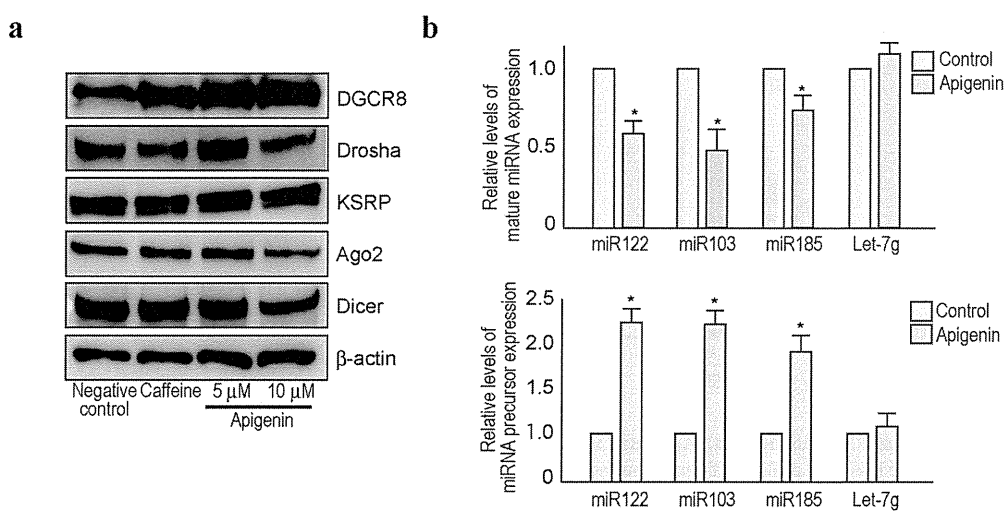

Figure 2 | Apigenin impairs miRNA maturation. (a), Cells were treated with the appropriate substances for 24 h and the indicated proteins were blotted. Representative results from three independent experiments using Huh7 cells are shown. Full-length blot images are available in Supplementary Figure 5a. (b), The expression levels of mature miRNAs and miRNA precursors were determined by qRT-PCR using Huh7 cells with or without apigenin treatment for 24 h. Data represent the means ± s.d. from three independent experiments. *, $p < 0.05$ (*t*-test) compared with the control (DMSO only) treatment.

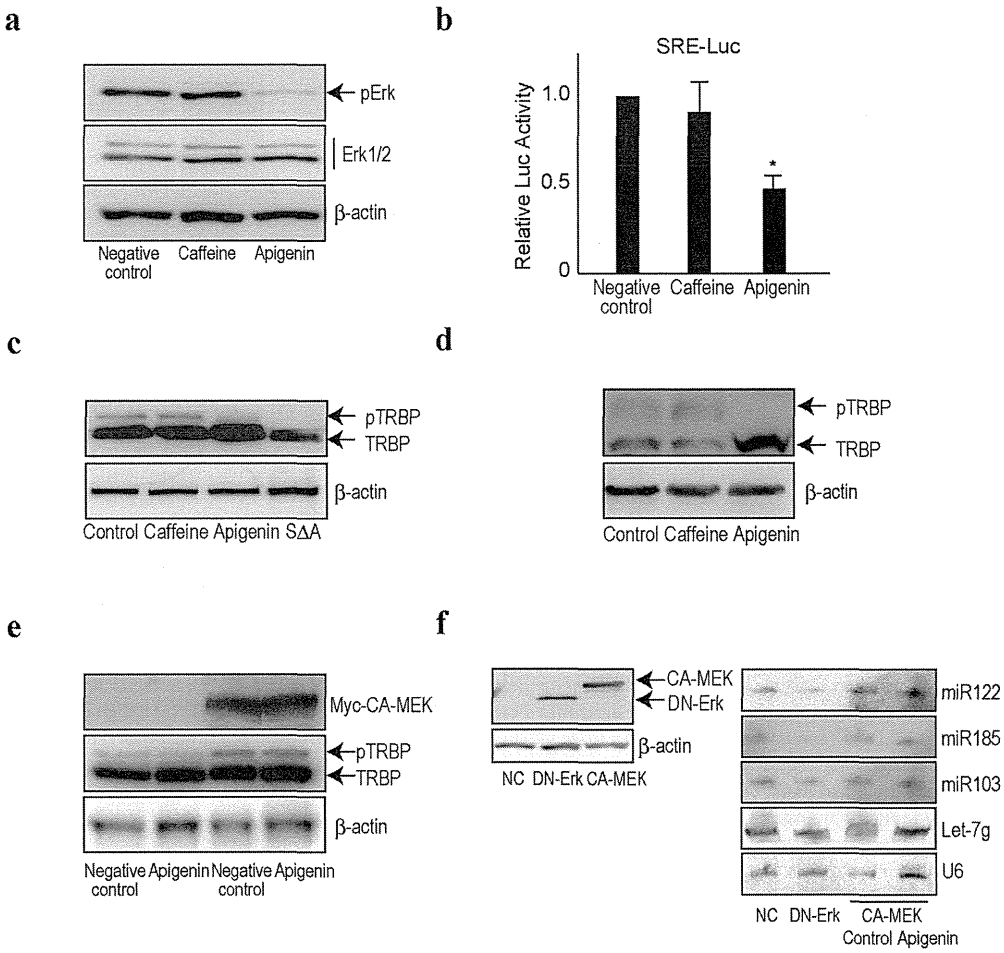

Figure 3 | Apigenin inhibits TRBP phosphorylation. (a), Cells were treated with caffeine or apigenin for 24 h. Cell lysates were blotted with anti-phosphorylated Erk and anti-total Erk1/2. Representative results from three independent experiments using Huh7 cells are shown. Similar results were obtained using Hep3B cells. (b), A luciferase assay was performed to determine SRE-driven transcription under apigenin treatment. Caffeine was included as a comparison. Data represent the means ± s.d. from three independent experiments using Huh7 cells. *, $p < 0.05$ (t-test) compared to the negative control. (c), Huh7 cells were transfected with wild-type TRBP-expressing plasmids followed by treatment with the indicated substances for 24 h. Serine-to-alanine mutant TRBP (SΔA) indicates non-phosphorylated TRBP. Representative results from three independent experiments using Huh7 cells are shown. (d), Substance-treated Huh7 cell lysates were separated using a Mn2+-Phos-tag gel to discriminate the phosphorylated form of TRBP. Representative results from three independent experiments using Huh7 cells are shown. (e), TRBP-expressing Huh7 cells were stably transfected with myc-tagged CA-MEK-expressing plasmids followed by apigenin treatment for 24 h. Phosphorylation status of TRBP was determined by Western blotting. Representative results from three independent experiments are shown. (f), Huh7 cells were stably transfected with myc-tagged CA-MEK-expressing plasmids or myc-tagged DN-Erk-expressing plasmids. The expression of the transfected constructs was confirmed by Western blotting using anti-myc antibodies (left panels). Expression levels of mature miRNAs in those cells with or without apigenin treatment were determined by Northern blotting (right panels). Representative results of at least three independent experiments are shown. Full-length blot images in a, b, c, d, e, and f are available in Supplementary Figure 5b, c, d, e, and f.

complexes due to overexpressing miR103 in these mice was confirmed by a lack of significant changes in the expression levels of other mature miRNAs, such as miR122 and miR185 (Figure 4a). As expected from a previous report[10], these miR103 transgenic mice showed an increase in both random and fasting blood-glucose levels and insulin levels (Supplementary Figure 3c and d). The mean size of adipocytes in visceral fat was larger in normal chow fed miR103 transgenic mice than in control mice, and their size became larger nearly in parallel in both control and miR103 transgenic mice under a high-fat diet (Supplementary Figure 3e).

To determine the effect of apigenin in these models, 40 mg/kg apigenin was intraperitoneally injected daily for 14 days in miR103 transgenic mice. The level of mature miR103 was decreased, and precursors accumulated in apigenin-treated mice, as determined by Northern blotting and qRT-PCR (Figure 4b and Supplementary Figure 4a and b). Similar to the in vitro results, levels of mature miR122 and miR185, but not let-7, in the liver tissues were also decreased by apigenin treatment (Supplementary Figure 4a and b). Phosphorylated TRBP in the liver tissues was decreased in apigenin-treated mice, as determined by a retarded band in the phos-tag gel (Figure 4c), consistent with the *in vitro* results (Figure 3d). Erk phosphorylation was consistently decreased following apigenin treatment (Supplementary Figure 4c). In addition, we confirmed the upregulated expression level of caveolin-1, a major regulator of the insulin receptor, which is a direct target gene of miR103[10] in these tissues (Supplementary Figure 4c). As expected from these results, apigenin-treated miR103 transgenic mice showed decreased random and fasting blood glucose-levels (Figure 4d). While miR103 transgenic mice

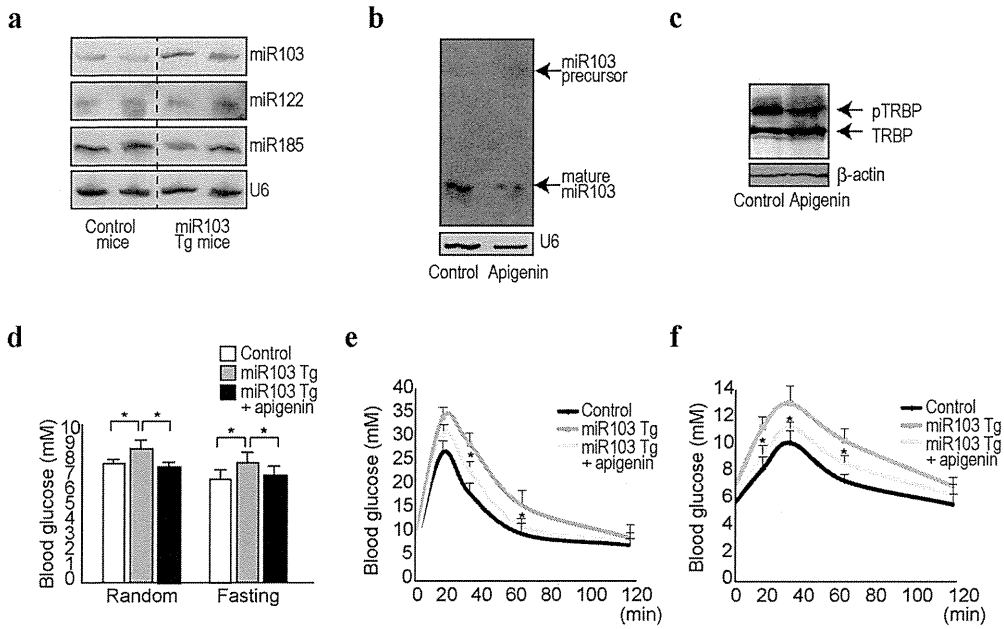

Figure 4 | Apigenin improves glucose tolerance in miR103 transgenic mice. (a), Expression levels of mature miR103, miR122, and miR185 in liver tissues of miR103 transgenic mice (miR103 Tg) were determined by Northern blotting. (b), Expression levels of mature miR103 and its precursor in liver tissues of miR10-transgenic mice treated with apigenin were determined by Northern blotting. Control (DMSO) or apigenin (40 mg/kg) was injected intraperitoneally daily for 14 days. Representative results from three independent mouse sets are shown. (c), Liver tissue homogenates from miR103 transgenic mice were separated using a phos-tag gel to determine the phosphorylation status of TRBP. Representative results from three independent mouse sets are shown. Full-length blot image is available in Supplementary Figure 5g. (d), Blood glucose levels were determined at random times or after 12 h fasting in control and miR103 transgenic (miR103 Tg) mice (n = 8 in each group). Data represent the means ± s.d. *, $p < 0.05$ (*t*-test). (e), (f), Glucose and pyruvate tolerance tests in control, miR103 transgenic (miR103 Tg), and miR103 transgenic with apigenin treatment (miR103 Tg + apigenin) mice (n = 6 in each group). Data represent the means ± s.d. *, $p < 0.05$ (*t*-test).

showed impaired glucose tolerance after an intraperitoneal glucose injection, apigenin treatment significantly suppressed these phenomena (Figure 4e). Similarly, while miR103 transgenic mice showed increased glucose production during an intraperitoneal pyruvate-tolerance test, apigenin treatment also suppressed these effects (Figure 4f). In addition, an increased number of small adipocytes and a decreased number of large adipocytes were observed in apigenin-treated miR103 transgenic mice (Supplementary Figure 3e and f). These results suggest that apigenin may have beneficial effects on pathological conditions in miR103 transgenic mice.

Discussion

In this study, we demonstrated that apigenin (4′,5,7-trihydroxyflavone) has inhibitory effects on the maturation processes of a subset of miRNAs and subsequent miRNA function. These effects may be mediated through inhibition of TRBP phosphorylation, possibly through inhibition of Erk activation. These results suggest that apigenin may be utilized to improve miRNA-mediated pathogenic states, such as glucose tolerance, induced by the over-expression of miRNA103.

Bioactive substances, such as caffeine and polyphenols, have been reported to have pleiotropic physiological effects[3,20]. However, those phenomena are descriptive in most cases and the underlying mechanisms are largely unclear. Apigenin, which is present in many fruits and vegetables, also has diverse biological effects, including improvement of the cancer cell response to chemotherapy[21], tumorigenesis[13,22], modulating immune cell function[23], and anti-platelet activity[24]. In this study, we showed that apigenin inhibits TRBP phosphorylation and its related miRNA maturation through inhibition of MAPK Erk activation. This modulation of miRNA function by apigenin may account, at least in part, for its various reported biological effects.

Phosphorylation of TRBP is mediated by Erk[15]. We showed clear inhibition of Erk phosphorylation by apigenin. Although previous studies have reported the inhibition of Erk activation by apigenin[16–19], the underlying mechanisms were unknown. Because Erk has many biological functions in intracellular signaling, modulation of TRBP phosphorylation and miRNA expression induced by Erk inhibition through apigenin is likely a part of the phenotype. To clarify the biological function of apigenin, identification of molecules on which apigenin directly acts must be the next step.

Another important finding in this study was the impaired glucose tolerance observed in miR103 transgenic mice. Previous studies showed that recombinant adenoviruses expressing the miR103/107 family (only one nucleotide difference in miR103 and miR107 at position 21) and a gain of miR103/107 function by transient infection in mice was sufficient to induce impaired glucose homeostasis, and these miRNAs play a central role in insulin sensitivity[10]. In this study, we confirmed that constitutive expression of miR103 in mice resulted in impaired glucose tolerance and increased size of adipocytes. These mice may represent a new *in vivo* model of metabolic disorders and facilitate development of new drugs targeting impaired glucose tolerance. In fact, we found that apigenin reversed impaired glucose tolerance in miR103-transgenic mice. Because apigenin is one of the flavonoids and is present in high content in celery and parsley, intake of apigenin from foods or dietary supplements may have some favorable effects on glucose intolerance induced by overexpression of miRNA levels, even if it does not completely overcome impaired glucose tolerance.

Phosphorylated TRBP is not related to the maturation of all miRNAs, but rather a subset of miRNAs[15]. With this respect, apigenin may have favorable effects on the pathogenic status induced by overexpression or overfunction of the miRNAs to which phosphorylated TRBP is related. Maturation of miR122, a liver-specific miRNA, is at least partly regulated by apigenin, as shown in our study, its crucial function in cholesterol synthesis[11,25–28], and hepatitis c viral replication[29,30]. Therefore, apigenin may also have beneficial effects on these conditions. Other effects of apigenin on the pathological state may be necessary to reconsider from the point of view of overexpression or overfunction of specific miRNAs.

Simultaneously, one should be cautious about the modulation of miRNA function by apigenin. Because some miRNAs may have favorable effects on human health, apigenin might be harmful if it inhibits the maturation and function of such miRNAs. For example, inhibitory effects on tumor-suppressive miRNAs should be avoided. Caution regarding these issues is necessary and, in parallel, the biological functions of miRNAs in general should be further examined.

In summary, we showed that apigenin displays inhibitory effects on the phosphorylation of TRBP and its subsequent miRNA maturation and function through regulation of Erk activity. Decreasing miRNA function may be used for treatment of conditions induced by over-functioning of miRNAs. Moreover, clarifying the as-yet-undiscovered functions of bioactive substances is important. Similar strategies to those used here may also be applied to other bioactive substances whose effects have been reported but the mechanisms are as yet undetermined.

Methods

Cell culture. The human hepatocellular carcinoma cell lines, Huh7 and Hep3B, were obtained from the Japanese Collection of Research Bioresources (JCRB, Osaka, Japan). All cells were maintained in Dulbecco's modified Eagle's medium supplemented with 10% fetal bovine serum.

Reagents. Caffeine, apigenin and chlorogenic acid were purchased from Wako Chemicals (Osaka, Japan). Procyanidin A2 and B2 were purchased from Indofine Chemical (Hillsborough, NJ) and ChromaDex (Irvine, CA). Caffeine, chlorogenic acid and procyanidin B2 were dissolved in water. Apigenin and procyanidin A2 were dissolved in dimethyl sulfoxide (DMSO). Caffeine, chlorogenic acid and procyanidin A2 and B2 were added at concentrations of 20 μM, 10 μM, 50 μg/mL, and 50 μg/mL, respectively, as reported previously[31–34]. Apigenin was used at 10 μM unless otherwise specified for *in vitro* studies, and 40 mg/kg was used for intraperitoneal injection daily for *in vivo* studies. An equal volume of DMSO only was used as a negative control.

Mouse experiments. Experimental protocols were approved by the Ethics Committee for Animal Experimentation at the Graduate School of Medicine, the University of Tokyo and the Institute for Adult Disease, Asahi Life Foundation, Japan and conducted in accordance with the Guidelines for the Care and Use of Laboratory Animals of the Department of Medicine, the University of Tokyo, and the Institute for Adult Disease, Asahi Life Foundation.

Plasmids, transfection and dual luciferase assays. Plasmids expressing miR122 and miR185 precursors and the corresponding firefly luciferase-based reporters have been described previously[8,35]. Plasmids expressing miRNA-103 precursors and the corresponding luciferase reporter were newly constructed according to protocols reported previously[8]. To determine MAPK pathway activity, SRE-driven luciferase was transfected, and dual luciferase assays were performed as described previously[9], with the exception that pGL4.74, a control plasmid containing *Renilla reniformis* (sea pansy) luciferase under control of the herpes simplex virus thymidine kinase promoter (Promega), was used as an internal control. Chemicals were added at 24 h and the reporter assays were done 48 h post-transfection. Constitutively active MEK1(DD) and dominant negative Erk(K/N) constructs with zeocin resistance genes were kindly provided by Prof. Takekawa (The Institute of Medical Sciences, the University of Tokyo)[36]. After transfection, the cells were selected with 6 μg/mL zeocin to establish cells stably expressing those constructs.

Western blot analysis. Protein lysates were prepared from cells or mouse liver tissues for immunoblotting analyses. Western blotting was performed as described previously[8]. Primary antibodies were purchased from Sigma (DGCR8, #SAB4200088; Dicer, #SAB4200087; TRBP2, #SAB4200111; β-actin, #A5441), Bethyl (KSRP, A302-021), Wako (Ago2, 015-22031), and Cell Signaling (Drosha, #D28B1; Phospho-Erk, #9101; Total Erk, #4695; myc-tag, #2276; Caveolin, #3267).

Northern blotting of miRNAs. Northern blotting of miRNAs was performed as described previously[9]. Briefly, total RNA was extracted using TRIzol Reagent (Invitrogen, Carlsbad, CA) according to the manufacturer's instructions. Ten micrograms of RNA were resolved in denaturing 15% polyacrylamide gels containing 7 M urea in 1× TBE and then transferred to a Hybond N+ membrane (GE Healthcare) in 0.25× TBE. Membranes were UV-crosslinked and prehybridized in hybridization buffer. Hybridization was performed overnight at 42°C in ULTRAhyb-Oligo Buffer (Ambion) containing a biotinylated probe specific for miR122 (CAA ACA CCA TTG TCA CAC TCC A), miR103 (TCA TAG CCC TGT ACA ATG CTG CT), miR185 (TCA GGA ACT GCC TTT CTC TCC A), and let-7g (AAC TGT ACA AAC TAC TAC CTC A), which had been heated to 95°C for 2 min. Membranes were washed at 42°C in 2× SSC containing 0.1% SDS, and the bound probe was visualized using a BrightStar BioDetect Kit (Ambion). Blots were stripped by boiling in a solution containing 0.1% SDS and 5 mM EDTA for 10 min prior to rehybridization with a U6 probe (CAC GAA TTT GCG TGT CAT CCT T).

Quantitative RT-PCR analysis of miRNA expression. To determine miR122, miR103, miR185, and let-7g expression levels, cDNA was first synthesized from RNA, and quantitative PCR was then performed using Mir-X miRNA First-Strand Synthesis and SYBR qRT-PCR Kit (Clontech). The expression levels of miRNA precursor were determined according to the previous report[37] using the reported primers. Relative expression values were calculated by the *CT*-based calibrated standard curve method. These calculated values were then normalized to the expression of U6 snRNA. The reverse primer was provided in the kit.

Determining TRBP phosphorylation status. Plasmids expressing wild-type TRBP and kinase-dead TRBP (TRBP SAA) were kindly provided by Professor Liu[15]. Twenty-four hours after transfection into Huh7 cells with corresponding plasmids, substances were treated for 24 h, and cell lysates were collected for subsequent Western blotting. To better discriminate the phosphorylated form of TRBP from the unphosphorylated form, a Mn2+-Phos-tag SDS-PAGE gel (Wako) was used according to the manufacturer's instructions.

Generation of miR103-expressing transgenic mice. To construct transgenic mice, plasmids expressing miRNA-103 precursors were modified as follows: to add the SV40 poly(A) tail signal downstream of the miR103 precursor sequences, the pCDH-miR103 precursor-expressing plasmid was digested at the *Not*I restriction site, and PCR-amplified poly(A) tail signal sequences were digested with *Cla*I from the original plasmid as a template was inserted by the Infusion cloning system (Clontech, Mountain View, CA). A DNA fragment of 1,125 bp, containing the CMV promoter region, the 470-bp genomic region for the miR103 precursor, and a SV40 poly(A) tail signal, was resected from the constructed plasmid by digestion with *Cla*I. Stable C57BL/6 embryonic stem (ES) cell lines were generated by electroporation of the linearized transgene, and the resulting cells were injected into blastocysts by the UNITECH Company (Chiba, Japan). Genotyping was performed by PCR using DNA isolated from tail snips. Four different mouse lines were maintained and the male littermates were used in the experiments.

Glucose test. Blood glucose was tested using a Glucose Pilot system (Iwai Chemical, Japan). Glucose tolerance and pyruvate tolerance tests were performed by intraperitoneal injection of glucose (2 g/kg) or pyruvate (2 g/kg) after fasting overnight. Blood glucose levels were measured before injection (0 min) and at 15, 30, 60, and 120 min after injection.

Adipocyte size. Visceral fat tissues stained with hematoxylin and eosin were analyzed using the Image-J software. One hundred adipocytes were measured per animal to determine adipocyte size. The high-fat diet was purchased from CLEA-Japan (Tokyo, Japan).

miRNA microarray analyses. miRNA microarray analysis was performed using miRNA oligo chips (Toray Industries, Tokyo, Japan). Normalization was performed using the intensities from U6, instead of the standard global normalization. The data and the protocols were deposited in a public database (Please refer the following link during the review process; http://www.ncbi.nlm.nih.gov/geo/query/acc.cgi?token=frwpxomkicoicte&acc=GSE46526).

Statistical analysis. Statistically significant differences between groups were determined using Student's *t*-test when variances were equal. When variances were unequal, Welch's *t*-test was used. *P*-values less than 0.05 were considered to indicate statistical significance.

1. Surh, Y. J. Cancer chemoprevention with dietary phytochemicals. *Nat Rev Cancer* **3**, 768–780 (2003).
2. D'Incalci, M., Steward, W. P. & Gescher, A. J. Use of cancer chemopreventive phytochemicals as antineoplastic agents. *Lancet Oncol* **6**, 899–904 (2005).
3. Baur, J. A. *et al.* Resveratrol improves health and survival of mice on a high-calorie diet. *Nature* **444**, 337–342 (2006).
4. Carrington, J. & Ambros, V. Role of microRNAs in plant and animal development. *Science* **301**, 336–338 (2003).
5. Bartel, D. P. MicroRNAs: genomics, biogenesis, mechanism, and function. *Cell* **116**, 281–297 (2004).
6. Ambros, V. The functions of animal microRNAs. *Nature* **431**, 350–355 (2004).

7. Lu, J. *et al.* MicroRNA expression profiles classify human cancers. *Nature* **435**, 834–838 (2005).
8. Kojima, K. *et al.* MicroRNA122 is a key regulator of α-fetoprotein expression and influences the aggressiveness of hepatocellular carcinoma. *Nat Commun* **2**, 338 (2011).
9. Takata, A. *et al.* MicroRNA-140 acts as a liver tumor suppressor by controlling NF-κB activity by directly targeting DNA methyltransferase 1 (Dnmt1) expression. *Hepatology* **57**, 162–170 (2013).
10. Trajkovski, M. *et al.* MicroRNAs 103 and 107 regulate insulin sensitivity. *Nature* **474**, 649–653 (2011).
11. Krützfeldt, J. *et al.* Silencing of microRNAs in vivo with 'antagomirs'. *Nature* **438**, 685–689 (2005).
12. Budhraja, A. *et al.* Apigenin induces apoptosis in human leukemia cells and exhibits anti-leukemic activity in vivo. *Mol Cancer Ther* **11**, 132–142 (2012).
13. Shukla, S. *et al.* Blockade of beta-catenin signaling by plant flavonoid apigenin suppresses prostate carcinogenesis in TRAMP mice. *Cancer Res* **67**, 6925–6935 (2007).
14. Wang, W. *et al.* Cell-cycle arrest at G2/M and growth inhibition by apigenin in human colon carcinoma cell lines. *Mol Carcinog* **28**, 102–110 (2000).
15. Paroo, Z., Ye, X., Chen, S. & Liu, Q. Phosphorylation of the human microRNA-generating complex mediates MAPK/Erk signaling. *Cell* **139**, 112–122 (2009).
16. Yi Lau, G. T. & Leung, L. K. The dietary flavonoid apigenin blocks phorbol 12-myristate 13-acetate-induced COX-2 transcriptional activity in breast cell lines. *Food Chem Toxicol* **48**, 3022–3027 (2010).
17. Tatsuta, A. *et al.* Suppression by apigenin of peritoneal metastasis of intestinal adenocarcinomas induced by azoxymethane in Wistar rats. *Clin Exp Metastasis* **18**, 657–662 (2000).
18. Yin, F., Giuliano, A. E. & Van Herle, A. J. Signal pathways involved in apigenin inhibition of growth and induction of apoptosis of human anaplastic thyroid cancer cells (ARO). *Anticancer Res* **19**, 4297–4303 (1999).
19. Kuo, M. L. & Yang, N. C. Reversion of v-H-ras-transformed NIH 3T3 cells by apigenin through inhibiting mitogen activated protein kinase and its downstream oncogenes. *Biochem Biophys Res Commun* **212**, 767–775 (1995).
20. Yao, S. L. *et al.* Selective radiosensitization of p53-deficient cells by caffeine-mediated activation of p34cdc2 kinase. *Nat Med* **2**, 1140–1143 (1996).
21. Chan, L. P. *et al.* Apigenin induces apoptosis via tumor necrosis factor receptor- and Bcl-2-mediated pathway and enhances susceptibility of head and neck squamous cell carcinoma to 5-fluorouracil and cisplatin. *Biochim Biophys Acta* **1820**, 1081–1091 (2012).
22. Mafuvadze, B., Liang, Y., Besch-Williford, C., Zhang, X. & Hyder, S. M. Apigenin induces apoptosis and blocks growth of medroxyprogesterone acetate-dependent BT-474 xenograft tumors. *Horm Cancer* **3**, 160–171 (2012).
23. Nicholas, C. *et al.* Apigenin blocks lipopolysaccharide-induced lethality in vivo and proinflammatory cytokines expression by inactivating NF-kappaB through the suppression of p65 phosphorylation. *J Immunol* **179**, 7121–7127 (2007).
24. Landolfi, R., Mower, R. L. & Steiner, M. Modification of platelet function and arachidonic acid metabolism by bioflavonoids. Structure-activity relations. *Biochem Pharmacol* **33**, 1525–1530 (1984).
25. Hsu, S. H. *et al.* Essential metabolic, anti-inflammatory, and anti-tumorigenic functions of miR-122 in liver. *J Clin Invest* **122**, 2871–2883 (2012).
26. Lanford, R. E. *et al.* Therapeutic silencing of microRNA-122 in primates with chronic hepatitis C virus infection. *Science* **327**, 198–201 (2010).
27. Elmén, J. *et al.* LNA-mediated microRNA silencing in non-human primates. *Nature* **452**, 896–899 (2008).
28. Esau, C. *et al.* miR-122 regulation of lipid metabolism revealed by in vivo antisense targeting. *Cell Metab* **3**, 87–98 (2006).
29. Jopling, C. L., Yi, M., Lancaster, A. M., Lemon, S. M. & Sarnow, P. Modulation of hepatitis C virus RNA abundance by a liver-specific MicroRNA. *Science* **309**, 1577–1581 (2005).
30. Lindow, M. & Kauppinen, S. Discovering the first microRNA-targeted drug. *J Cell Biol* **199**, 407–412 (2012).
31. Ku, B. M. *et al.* Caffeine inhibits cell proliferation and regulates PKA/GSK3β pathways in U87MG human glioma cells. *Mol Cells* **31**, 275–279 (2011).
32. Nishizuka, T. *et al. Procya* nidins are potent inhibitors of LOX-1: a new player in the French Paradox. *Proc Jpn Acad Ser B Phys Biol Sci* **87**, 104–113 (2011).
33. Teraoka, M. *et al.* Cytoprotective effect of chlorogenic acid against α-synuclein-related toxicity in catecholaminergic PC12 cells. *J Clin Biochem Nutr* **51**, 122–127 (2012).
34. Shukla, S. & Gupta, S. Apigenin: a promising molecule for cancer prevention. *Pharm Res* **27**, 962–978 (2010).
35. Takata, A. *et al.* MicroRNA-22 and microRNA-140 suppress NF-κB activity by regulating the expression of NF-κB coactivators. *Biochem Biophys Res Commun* **411**, 826–831 (2011).
36. Kubota, Y., O'Grady, P., Saito, H. & Takekawa, M. Oncogenic Ras abrogates MEK SUMOylation that suppresses the ERK pathway and cell transformation. *Nat Cell Biol* **13**, 282–291 (2011).
37. Suzuki, H. I. *et al. Modulat* ion of microRNA processing by p53. *Nature* **460**, 529–533 (2009).

Acknowledgments

This work was supported by Grants-in-Aid from the Ministry of Education, Culture, Sports, Science and Technology, Japan (#25293076 and #24390183) (to M. Otsuka and K. Koike), by Health Sciences Research Grants of The Ministry of Health, Labor and Welfare of Japan (to K. Koike), and grants from the Nestlé Nutrition Council, Japan (to A.T.), and the Foundation of All Japan Coffee Association (to M. Otsuka).

Author contributions

M.Ohno, C.S. and M.Otsuka planned the research and wrote the paper. M.Ohno, C.S., T.K., T.Y., A.T., K.Kojima, and M.Otsuka performed the majority of the experiments. M.A. and H.Y. contributed materials. Y.K. supported several experiments. K.Koike supervised the entire project.

Additional information

Supplementary information accompanies this paper at http://www.nature.com/scientificreports

Competing financial interests: The authors declare no competing financial interests.

How to cite this article: Ohno, M. *et al.* The flavonoid apigenin improves glucose tolerance through inhibition of microRNA maturation in miRNA103 transgenic mice. *Sci. Rep.* 3, 2553; DOI:10.1038/srep02553 (2013).

Hepatology Research

Hepatology Research 2013; 43: 596–604 doi: 10.1111/j.1872-034X.2012.01115.x

Original Article

Fibrosis score consisting of four serum markers successfully predicts pathological fibrotic stages of chronic hepatitis B

Kenji Ikeda,[1,2] Namiki Izumi,[3] Eiji Tanaka,[7] Hiroshi Yotsuyanagi,[4] Yoshihisa Takahashi,[5] Junichi Fukushima,[6] Fukuo Kondo,[5] Toshio Fukusato,[5] Kazuhiko Koike,[4] Norio Hayashi[8] and Hiromitsu Kumada[1,2]

[1]Department of Hepatology, Toranomon Hospital, [2]Okinaka Memorial Institute for Medical Research, [3]Department of Gastroenterology, Musashino Red Cross Hospital, [4]Department of Gastroenterology, Tokyo University of Medicine,[5]Department of Pathology, Teikyo University School of Medicine, [6]Department of Pathology, NTT Medical Center Tokyo, Tokyo, [7]Department of Gastroenterology, Shinshu University of Medicine, Matsumoto, and [8]Department of Gastroenterology, Kansai-Rosai Hospital, Hyogo, Japan

Aim: In order to evaluate and judge a fibrotic stage of patients with chronic hepatitis B, multivariate regression analysis was performed using multiple fibrosis markers.

Method: A total of 227 patients from seven hepatology units and institutes were diagnosed by needle biopsy as having chronic liver disease caused by hepatitis B virus. Twenty-three variables and their natural logarithmic transformation were employed in the multivariate analysis. Multiple regression function was generated from data of 158 patients in one hospital, and validation was performed using the other data of 69 patients from six other hospitals.

Results: After stepwise variable selection, multivariate regression analysis finally obtained the following function: $z = 1.40 \times ln$ (type IV collagen 7S) (ng/mL) $- 0.017 \times$ (platelet count) ($\times 1000^3/mm^3$) $+ 1.24 \times ln$ (tissue inhibitor of matrix metalloproteinase-2) (ng/mL) $+ 1.19 \times ln$ (α-2-macroglobulin) (mg/dL) $- 9.15$. Median values of fibrosis scores of F1 ($n = 73$), F2 ($n = 42$), F3 ($n = 31$) and F4 stages ($n = 12$) were calculated as 0.95, 2.07, 2.98 and 3.63, respectively. Multiple regression coefficient and coefficient of determination were 0.646 and 0.418, respectively. Validation with patient data from other institutions demonstrated good reproducibility of fibrosis score for hepatitis B (FSB), showing 1.33 in F1 ($n = 27$), 2.20 in F2 ($n = 20$), 3.11 in F3 ($n = 20$) and 5.30 in F4 ($n = 2$), respectively.

Conclusion: A concise multiple regression function using four laboratory parameters successfully predicted pathological fibrosis stage of patients with hepatitis B virus infection.

Key words: chronic hepatitis, hepatitis B virus, liver cirrhosis, liver fibrosis, multiple regression analysis, stage

INTRODUCTION

WHEN HEPATITIS B virus (HBV)-related chronic liver disease is found by biochemical and virological examination, liver biopsy can establish the definitive diagnosis of chronic hepatitis and its fibrotic staging. Although these pathological procedures are reliable and informative both in diagnosis and treatment, they sometimes require medical invasion and financial costs, including the risk of bleeding from needle puncture, some pain experienced during the procedure and hospital stays of a few days. The pathological examination is, therefore, rarely performed repeatedly in a short period of time, unless disease activity is severe or progression of liver disease is highly suspected. Recently, many authors described the usefulness of ultrasonographic elastography and multiple resonance imaging technology in the estimation of staging of chronic hepatitis and cirrhosis.[1–5] These ways of estimation using the imaging apparatuses seem truly useful for current patients, but they cannot evaluate and compare with past fibrotic states of patients retrospectively. Moreover,

Correspondence: Dr Kenji Ikeda, Department of Hepatology, Toranomon Hospital, 2-2-2 Toranomon, Minato-ku, Tokyo, 105-8470, Japan. Email: ikedakenji@tora.email.ne.jp
Received 6 May 2012; revision 17 September 2012; accepted 4 October 2012.

the same apparatus for elastometry will not be available for repeated measurement for a follow-up examination, for example, several years later.

In spite of the accuracy of biopsy and convenience of elastography in chronic liver disease, clinical diagnosis based on biochemistry and hematology is still indispensable for the daily practice of many patients with HBV-related liver disease. Recently, several studies were published about estimation of hepatitis stages, using one or more serum biomarkers. Discriminant functions or multivariate analyses demonstrated that approximately 60–90% of patients with chronic hepatitis B were correctly classified as having mild hepatitis and severe hepatitis with advanced fibrosis.[2,6–13] Up to the present time, however, the usefulness of the discriminant functions are less valuable for a few reasons. First, these functions were made for the purpose of discrimination of severe hepatic fibrosis from mild fibrosis, and four histological classifications (F1–F4) were neglected in almost of the studies. Second, some studies analyzed both hepatitis B and hepatitis C virus infection, although the significance and actual values of each liver function test in the evaluation of the severity of liver disease were not similar among each viral hepatitis and alcoholic liver disease. Third, biochemical markers for liver fibrosis (e.g. hyaluronic acid, type IV collagen, procollagen III peptide)[14–16] were not always included in those previous studies.

We tried to generate a function estimating fibrotic stages of HBV-related chronic hepatitis, which were objectively diagnosed by liver biopsy. The purpose of this study is, therefore, to make a reliable multiple regression function and to obtain practical coefficients for significant variables also using fibrosis markers.

METHODS

Patients

A TOTAL OF 273 Japanese patients with chronic hepatitis B were recruited for the study from seven hospitals in Japan: Toranomon Hospital, Hiroshima University Hospital (K. Chayama, M.D.), Ehime University Hospital (M. Onji, M.D.), Musashino Red Cross Hospital (N. Izumi, MD), Shishu University Hospital (E. Tanaka, M.D.), Showa University Hospital (M. Imawari, M.D.) and Osaka University Hospital (T. Takehara, M.D.). Inclusion criteria for this study were: (i) positive hepatitis B surface antigen for more than 6 months; (ii) persistent or intermittent elevation in aspartate aminotransferase (AST)/alanine aminotransferase (ALT) levels; and (iii) liver biopsy showing chronic hepatitis (F1–F4). We excluded those patients with overt alcoholic liver disease or fatty liver, association of other types of liver disease (e.g. hepatitis C, primary biliary cirrhosis, autoimmune hepatitis), or those associated with hepatocellular carcinoma or other malignancy. Among the patients, 244 patients fulfilled the conditions for the study: complete demographic data, basic laboratory data of hematology and biochemistry, required liver biopsy specimens, and sufficient amount of frozen sera. Also, we excluded additional 17 patients with eventual histological diagnosis as F0 stage.

Finally, a total of 227 patients who were diagnosed as having chronic hepatitis or cirrhosis (F1–F4) were analyzed for the following hematological, biochemical and histopathological examination. There were 172 males and 55 females aged 16–70 years (median, 39 years).

All the patients presented written informed consent in individual hospitals and medical centers, and the study was approved in each ethical committee.

Hematological and biochemical examination

Hematological and standard biochemical evaluation had been performed in each medical institution: white blood cells, red blood cells, hemoglobin, platelets, total bilirubin, AST, ALT, AST/ALT ratio (AAR), γ-glutamyl transpeptidase (γ-GTP), total protein, albumin and γ-globulin.

Special biochemical examinations including "fibrosis markers" were carried out using stored frozen sera at −20°C or lower: α-2-macroglobulin, haptoglobin concentration, haptoglobin typing, apolipoprotein A1, hyaluronic acid, tissue inhibitor of matrix metalloproteinase (TIMP)-1, TIMP-2, procollagen III peptide and type IV collagen 7S.

Histological diagnosis of chronic hepatitis and cirrhosis

All the 227 cases fulfilled required standards of histological evaluation: sufficient length of specimen, hematoxylin–eosin staining, and at least one specimen with fiber staining. Four independent pathologists (Y. T., J. F., F. K. and T. F.), who were not informed of patients' background and laboratory features except for age and sex, evaluated the 227 specimens regarding the stages of fibrosis and activity. Pathological classification of chronic hepatitis staging was based on Desmet *et al.*[17]

Before judgment of histological staging of individual specimens, the pathologists discussed the objective and reproducible judgment of pathological diagnosis of

hepatitis. They made a panel about obvious criteria using typical microscopic pictures for each stage, and it was always referred to during the procedure of pathological judgment. When inconsistent results were found in the diagnosis of hepatitis stage among the pathologists, the final judgment accepted majority rule among them.

Statistical analysis

Non-parametric procedures were employed for the analysis of background characteristics and laboratory data among patients in each stage, including Mann–Whitney *U*-test, Kruskal–Wallis test and χ^2-test.

The normality of the distribution of the data was evaluated by a Kolmogorov–Smirnov one-sample test. Because certain variables partly did not conform to a normal distribution, natural logarithmic transformation of bilirubin, AST, ALT, γ-GTP, α-2-macroglobulin, hyaluronic acid, type IV collagen 7S and TIMP-2 were also analyzed in the following calculation. The natural logarithmic transformation of the results yielded a normal distribution or symmetrical distribution for all the analyzed factors. After the procedures, the following multiple regression analysis became rationally robust against deviations from normal distribution. In order to avoid introducing into the model any variables that were mutually correlated, we checked the interaction between all pairs of the variables by calculating variance inflation factors. Of the highly correlated variables, less significant factors were removed from the viewpoint of multicollinearity.

Multivariate regression analysis was performed using 158 patient data from Toranomon Hospital (training dataset) to generate a training data of predicting function. We used a stepwise method for selection of informative subsets of explanatory variables in the model. Multiple regression coefficient and coefficient of determination were also taken into account in the selection of variables. Next, we validated the obtained predictive function using the remaining 69 patient data from the other six liver institutions (validation dataset).

A *P*-value of less than 0.05 with two-tailed test was considered to be significant. Data analysis was performed using the computer program SPSS ver. 19.[18]

For evaluation of the efficiency and usefulness of obtained function for fibrosis estimation, we compared various fibrosis scores for hepatitis B and C, including AAR,[19] AST-to-platelet ratio index (APRI),[20] FIB-4,[21] FibroTest[22] and discrimination function of cirrhosis from hepatitis in Japanese patients.[23]

RESULTS

Pathological diagnosis

FOUR PATHOLOGISTS INDEPENDENTLY judged the fibrotic stages and inflammatory activity for 227 specimens of chronic hepatitis/cirrhosis caused by HBV. One hundred patients (44.1%) had a fibrosis stage of F1, 62 (27.3%) F2, 51 (22.5%) F3 and 14 (6.2%) F4. In the subgroup of the 158 patients in the training group, judgment as F1 was made in 73 cases, F2 in 42, F3 in 31 and F4 in 12. Of the 69 patients in the validation group, judgment as F1 was made in 27, F2 in 20, F3 in 20 and F4 in two.

According to hepatitis activity classification, A0 was found in five (2.2%), A1 in 100 (44.1%), A2 in 107 (47.1%) and A3 in 15 (6.6%).

Laboratory data of each hepatitis stage in the training group

There were 124 men and 34 women with a median age of 39 years ranged 16–70 years. Laboratory data of 158 patients in the training group are shown in Table 1. Although several individual items were well correlated with the severity of hepatic fibrosis, significant overlap values were noted among F1–F4 stages: platelet count, γ-globulin, α-2-macroglobulin, haptoglobin, hyaluronic acid, TIMP-2 and type IV collagen 7S.

Significant variables serving staging of hepatitis

Univariate analyses using trend analysis with the Cochran–Armitage method showed that the fibrotic stage of chronic hepatitis B (FSB) was significantly correlated with platelet count (Spearman: $r = -0.45$, $P < 0.001$), γ-GTP ($r = 0.19$, $P = 0.017$), γ-globulin ($r = 0.29$, $P < 0.001$), α-2-macroglobulin ($r = 0.32$, $P < 0.001$), hyaluronic acid ($r = 0.36$, $P < 0.001$), TIMP-2 ($r = 0.16$, $P = 0.043$), procollagen III peptide ($r = 0.30$, $P < 0.001$) and type IV collagen 7S ($r = 0.55$, $P < 0.001$).

Regression function generated from training patient group

After stepwise variable selection, multivariate regression analysis finally obtained the following function: $z = 1.40 \times ln$ (type IV collagen 7S) (ng/mL) $- 0.017 \times$ (platelet count) ($\times 1000^3/mm^3$) $+ 1.24 \times ln$ (TIMP-2) (ng/mL) $+ 1.19 \times ln$ (α-2-macroglobulin) (mg/dL) $-$ 9.15. Median values of the fibrosis score of F1 ($n = 73$), F2 ($n = 42$), F3 ($n = 31$) and F4 stages ($n = 12$) were calculated as 0.95, 2.07, 2.98 and 3.63, respectively

Table 1 Demography and laboratory data of 158 patients in training group

	F1 ($n = 73$)	F2 ($n = 42$)	F3 ($n = 31$)	F4 ($n = 12$)
Demographics				
Men : women	58:15	33:9	23:8	10:2
Age (median, range)	36 (16–70)	39.5 (18–66)	39 (25–64)	43 (32–59)
Laboratory data (median, range)				
WBC (×1000/mm^3)	5.4 (2.5–10.6)	5.1 (2.4–8.7)	4.9 (3.0–8.7)	4.1 (3.7–6.6)
Hemoglobin (g/dL)	15.3 (10.3–18.8)	15.4 (12.5–17.9)	15.2 (11.5–17.2)	14.45 (12.1–18.2)
Platelet (×1000/mm^3)	204 (124–341)	173 (82–308)	155 (96–220)	130 (86–230)
Albumin (g/dL)	4.1 (3.2–4.9)	4.0 (3.2–5.1)	4.0 (3.3–4.9)	3.95 (3.4–4.6)
Bilirubin (mg/dL)	0.8 (0.2–1.7)	0.8 (0.3–2.3)	0.9 (0.4–5.4)	0.85 (0.6–2.3)
AST (IU/L)	48 (16–450)	55 (17–588)	54 (17–1446)	76.5 (27–396)
ALT (IU/L)	102 (10–839)	90 (12–886)	85 (19–2148)	89 (18–809)
γ-GTP (IU/L)	37 (7–247)	55 (8–687)	44 (14–564)	69 (33–262)
γ-Globulin (g/dL)	1.29 (0.78–2.11)	1.495 (0.62–3.20)	1.43 (0.90–2.30)	1.735 (0.92–2.47)
γ-Globulin (%)	17.3 (10.8–26.1)	19.3 (8.5–35.6)	19.9 (12.9–28.6)	22.55 (13.9–30.2)
α-2-Macroglobulin (mg/dL)	226 (116–446)	276 (148–495)	261 (202–565)	286.5 (166–425)
Haptoglobin (mg/dL)	77 (<5–318)	59 (<5–238)	61 (<5–151)	48.5 (<5–145)
Apolipoprotein A-I (mg/dL)	134 (89–212)	143 (78–250)	133 (87–189)	125 (73–169)
Hyaluronic acid (μg/L)	16 (<5–130)	32.5 (<5–204)	38 (<5–418)	49 (24–335)
TIMP-1 (ng/mL)	168 (93–271)	172 (116–314)	157 (119–365)	192 (145–365)
TIMP-2 (ng/mL)	80 (41–135)	80.5 (35–121)	92 (38–251)	85.5 (70–123)
Procollagen III peptide (U/mL)	0.75 (0.53–1.90)	0.835 (0.45–1.20)	0.89 (0.58–2.50)	1.05 (0.71–2.20)
Type IV collagen 7S (ng/ml)	4.0 (2.7–7.7)	4.6 (2.6–9.6)	5.6 (2.3–15.0)	7.2 (4.2–14.0)

ALT, alanine aminotransferase; AST, aspartate aminotransferase; γ-GTP, γ-glutamyl transpeptidase; TIMP, tissue inhibitor of matrix metalloproteinase; WBC, white blood cells.

(Fig. 1). The multiple regression coefficient and coefficient of determination were 0.646 ($P < 0.001$) and 0.418 ($P < 0.001$), respectively.

Because the generated regression function was obtained by multivariate analysis with stepwise variable selection, several variables were removed from the function due to multicollinearity among them. Mutual correlation among the fibrosis predictors are shown in Table 2.

A 28-year-old man of F1 fibrotic stage (Fig. 2a) had a serum type IV collagen concentration of 4.4 ng/mL, platelet 221 × 10^3 count/mm^3, TIMP-2 75 ng/mL and α-2-macroglobulin 226 mg/dL. The regression function provided a fibrosis score of 0.99. Another man aged 46 years had F3 fibrosis on histological examination (Fig. 2b). His type IV collagen was 5.3 ng/mL, platelet 137 × 10^3 count/mm^3, TIMP-2 92 ng/mL and α-2-macroglobulin 255, and the regression function calculated his fibrosis score as 3.10.

Validation of discriminant function

Validation data of 69 patients (Table 3) were collected from the other six institutions in Japan. When applying

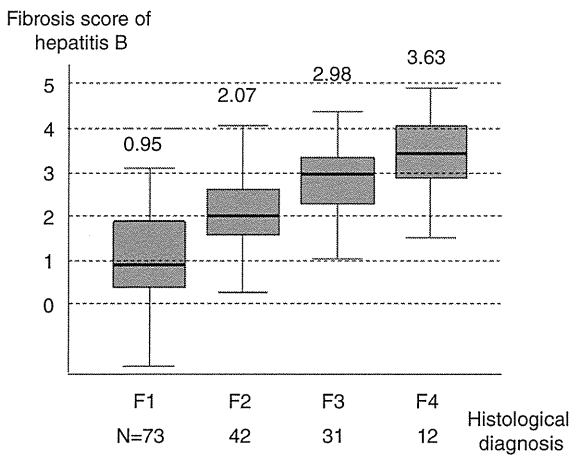

Figure 1 Box and whisker plots of fibrotic score of each histological fibrosis group in the training dataset. The fibrosis score of hepatitis B was generated by the function, $z = 1.40 \times ln$ (type IV collagen 7S) (ng/mL) − 0.017 × (platelet count) (×1000^3/mm^3) + 1.24 × *ln* (tissue inhibitor of matrix metalloproteinase-2) (ng/mL) + 1.19 × *ln* (α-2-macroglobulin) (mg/dL) − 9.15.

Table 2 Correlation coefficients (Spearman's ρ) among fibrosis predictors used in multivariate analysis

	Platelet	gamma-globulin	*ln* (α-2-macroglobulin)	*ln* (hyaluronate)	*ln* (P-III-P)	*ln* (IV collagen)	*ln* (TIMP-2)
Platelet ($\times 10^3/mm^3$)	1.000	−0.214 ($P = 0.008$)	−0.260 ($P = 0.001$)	−0.384 ($P < 0.001$)	−0.045 ($P = 0.58$)	−0.297 ($P < 0.001$)	0.094 ($P = 0.24$)
γ-Globulin (g/dL)		1.000	0.276 ($P = 0.001$)	0.349 ($P < 0.001$)	0.342 ($P < 0.001$)	0.414 ($P < 0.001$)	0.268 ($P = 0.001$)
ln (α-2-macroglobulin) (mg/dL)			1.000	0.281 ($P < 0.001$)	0.141 ($P = 0.078$)	0.171 ($P = 0.032$)	−0.079 ($P = 0.32$)
ln (hyaluronic acid) (mg/L)				1.000	0.373 ($P < 0.001$)	0.493 ($P < 0.001$)	0.089 ($P = 0.27$)
ln (procollagen III peptide) (U/mL)					1.000	0.600 ($P < 0.001$)	0.145 ($P = 0.071$)
ln (type IV collagen) (mg/L)						1.000	0.358 ($P < 0.001$)
ln (TIMP-2) (mg/L)							1.000

TIMP, tissue inhibitor of matrix metalloproteinase.

the regression function for the validation set, the fibrosis score demonstrated good reproducibility, showing 1.33 in patients with chronic hepatitis of F1 ($n = 27$), 2.20 of F2 ($n = 20$), 3.11 of F3 ($n = 20$) and 5.30 of F4 ($n = 2$), respectively (Fig. 3). Although F4 fibrosis stage consisted of only two patients and the score 5.30 was regarded as of rather higher value, the scores of other stages of fibrosis were concordant with histological fibrosis.

Comparisons of efficacy with various fibrosis scores (Fig. 4)

In order to evaluate the efficacy and usefulness of the obtained FSB, we compared it with previously reported fibrosis scores using training data. AAR, APRI and FibroTest showed only slight correlation with actual histological stage. FIB-4 demonstrated an increasing trend of the score associated with histological fibrosis, but significant overlapping scores were found in F1–F4. Spearman's correlation coefficients of AAR, APRI, FIB-4 and FibroTest were 0.199 ($P = 0.012$), 0.265 ($P = 0.001$), 0.412 ($P < 0.001$) and 0.330 ($P < 0.001$), respectively. Our FSB showed a Spearman's correlation coefficient of 0.625 ($P < 0.001$), and was a much higher value than the others. The dichotomous discrimination function for cirrhosis and hepatitis C in Japanese patients[23] showed good differentiation also in patients with hepatitis B virus.

DISCUSSION

RECOGNITION OF SEVERITY of chronic hepatitis is essential in managing patients with chronic HBV infection: estimation of length of infection, existence of any previous hepatitis activity, presumption of current fibrotic stage, and prediction of future fibrosis progression and hepatocarcinogenesis. Differential diagnosis of cirrhosis from chronic hepatitis is especially important in the evaluation of chronic HBV infection. Identification of liver cirrhosis often leads to an important change in management of the patient: need for fiberscopic examination for esophageal varices, ultrasonographic exploration for the association of liver cancer, and prediction of hepatic decompensation. Guidelines published by the American Association of Study of Liver Disease[24] recommend liver biopsy for HBV carriers with aminotransferase elevation or for any candidates of antiviral therapy, because hepatic fibrosis sometimes shows unexpectedly far advancement to cirrhosis, and because it is very difficult to evaluate and translate the liver function tests or ultrasonographic findings compared to chronic hepatitis type C.

Table 3 Demography and laboratory data of 69 patients in training group

	F1 ($n = 27$)	F2 ($n = 20$)	F3 ($n = 20$)	F4 ($n = 2$)
Demographics				
Men : women	18:9	15:5	13:7	2:0
Age (median, range)	36 (13–64)	45 (14–64)	36.5 (24–59)	32 (25–39)
Laboratory data (median, range)				
WBC (×1000/mm^3)	5.0 (2.8–8.7)	5.8 (2.8–11.6)	5.3 (3.2–8.1)	3.85 (2.7–5.0)
Hemoglobin (g/dL)	14.8 (12.4–17.4)	15.0 (12.4–16.9)	14.4 (11.1–16.4)	14.4 (12.5–16.3)
Platelet (×1000/mm^3)	204 (86–322)	180 (90–275)	147 (90–276)	130 (67–183)
Albumin (g/dL)	4.4 (2.8–5.2)	4.2 (3.5–5.1)	4.3 (3.4–4.9)	4.45 (4.0–4.9)
Bilirubin (mg/dL)	0.9 (0.4–6.4)	0.8 (0.2–1.6)	0.75 (0.4–1.7)	1.15 (1.1–1.2)
AST (IU/L)	52 (17–575)	50.5 (21–272)	65 (22–284)	248.5 (51–446)
ALT (IU/L)	84 (16–1101)	101.5 (19–554)	86.5 (16–1113)	453.5 (74–833)
γ-GTP (IU/L)	42 (14–332)	54 (16–205)	52.5 (13–191)	193 (57–329)
γ-Globulin (g/dL)	1.30 (1.04–1.59)	1.35 (1.18–2.53)	1.62 (1.16–1.97)	1.545 (1.51–1.58)
γ-Globulin (%)	17.9 (14.3–22.1)	19.6 (15.5–30.8)	22.0 (16.5–24.6)	20.15 (19.3–21.0)
α-2-Macroglobulin (mg/dL)	287 (160–687)	270 (89–452)	272.5 (211–463)	389 (313–465)
Haptoglobin (mg/dL)	58 (<5–229)	74 (<5–154)	56.5 (<5–198)	<5 (<5–<5)
Apolipoprotein A-I (mg/dL)	146 (95–216)	137 (87–162)	120 (88–170)	100.5 (74–127)
Hyaluronic acid (μg/L)	27 (<5–113)	36 (10–1050)	59 (14–439)	331 (225–437)
TIMP-1 (ng/mL)	168.5 (83–302)	176 (127–408)	182 (104–303)	390.5 (283–498)
TIMP-2 (ng/mL)	76 (25–143)	86.5 (28–154)	77.5 (32–141)	100.5 (91–110)
Procollagen III peptide (U/mL)	0.71 (0.27–2.20)	0.88 (0.63–2.80)	0.995 (0.60–2.10)	1.75 (1.50–2.00)
Type IV collagen 7S (ng/ml)	3.6 (2.7–17.0)	5.25 (3.3–13.0)	5.7 (3.0–16.0)	15.5 (15.0–16.0)

ALT, alanine aminotransferase; AST, aspartate aminotransferase; γ-GTP, γ-glutamyl transpeptidase; TIMP, tissue inhibitor of matrix metalloproteinase; WBC, white blood cells.

Recently, non-invasive estimation of severity of liver fibrosis has been reported in patients with HBV-related chronic hepatitis.[2,6–13] However, these studies were principally aimed at differentiation of advanced fibrotic stages of F3 or F4 from mild fibrotic stages of F1 or F2. Those discrimination functions were insufficient to recognize the stepwise progression of viral hepatitis from F1–F4. This dichotomy (mild or severe) of chronic hepatitis B seemed less valuable in the study of disease progression, disease control abilities of antiviral drugs and estimation of histological improvement after anti-inflammatory drugs. A histology-oriented, practical and reliable formula is therefore required for the diagnosis and investigation of chronic hepatitis B.

This study aimed to establish non-invasive evaluation and calculation of liver fibrosis for patients with chronic hepatitis B virus infection. Although it was retrospectively performed as a multicenter study of eight institutions, judgment of histological diagnosis was independently performed by four pathologists in another hospital, who were informed only of the patient's age, sex and positive HBV infection. Objective judgment of the histological staging and grading in sufficient biopsy specimens could be obtained.

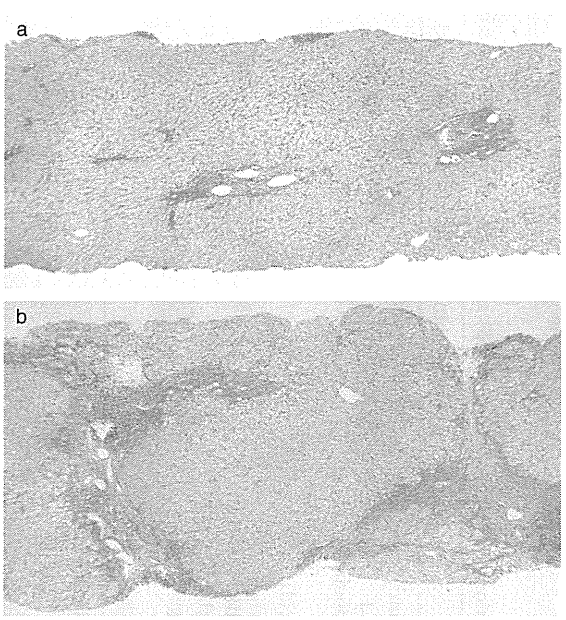

Figure 2 Case presentations of the training set. (a) A 28-year-old man with F1 fibrosis. Final regression function provided his fibrosis score as 0.99. (b) A 45-year-old man with F3 fibrosis. His regression coefficient was calculated as 3.10. Silver stain, ×40.

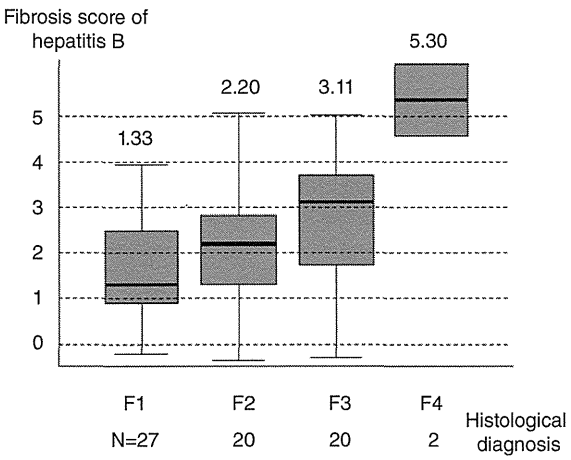

Figure 3 Box and whisker plots of fibrotic score of each group of histological fibrosis in the validation dataset. The fibrosis score of hepatitis B was generated by the function, $z = 1.40 \times ln$ (type IV collagen 7S) (ng/mL) − $0.017 \times$ (platelet count) ($\times 1000^3/mm^3$) + $1.24 \times ln$ (tissue inhibitor of matrix metalloproteinase-2) (ng/mL) + $1.19 \times ln$ (α-2-macroglobulin) (mg/dL) − 9.15.

As many as 227 patients with chronic hepatitis B were analyzed in this study, who had been diagnosed as having chronic hepatitis or cirrhosis by liver biopsy performed in experienced liver units in Japan. To obtain the most suitable equation approximating histological fibrotic stage, multivariate analysis was performed using two demographic parameters (age and sex) and 21 hematological and biochemical markers with or without logarithmic transformation. They included many kinds of fibrosis markers: α-2-macroglobulin, haptoglobin concentration, haptoglobin typing, apolipoprotein A1, hyaluronic acid, TIMP-1, TIMP-2, procollagen III peptide and type IV collagen 7S Multiple regression analysis finally generated a first-degree polynomial function consisting of four variables: type IV collagen 7S, platelet count, TIMP-2 and α2-macroglobulin. A constant numeral (−9.15) was finally adjusted in the regression equation in order to obtain fitted figures for a fibrotic stage of F1–F4. From the magnitude of the standardized partial regression coefficient of individual variable in the function, platelet count demonstrated the most potent contribution toward the prediction of liver fibrosis. Type IV collagen 7S and *ln* (TIMP-2) proved to be the second and third distinctive power in the model, respectively.

The FSB was sufficiently fitted to actual fibrotic stages with certain overlapping as is usually found in histological ambiguity judged by pathologists. Because judgment of fibrosis in chronic hepatitis often shows a transitional histological staging, pathological examination cannot always make a clear-cut diagnosis discriminating F1–F4. Considering the limitation of the pathological difficulty in differentiating the four continuous disease entities, the obtained regression function showed satisfactory high accuracy rates in the prediction of liver disease severity. The FSB can provide one or two decimal places (e.g. 3.2 or 3.24) and the utility of the score is possibly higher than the mere histological stage of F1–F4. The reproducibility was confirmed by the remaining 67 patients' data obtained from the other six hospitals. Although the validation data were collected from a different geographic area and different chronological situation, the FSB showed similar results in prediction of histological staging.

The FSB seemed a very useful quantitative marker in evaluating fibrotic severity of hepatitis B patients without invasive procedures and without any specialized ultrasonography or magnetic resonance imaging. The FSB also has an advantage of measurement, in which old blood samples are available for retrospective assessment of varied clinical settings: for example, old sera from 20 years prior to the time of initial liver biopsy, or paired sera before and after long-term antiviral therapy. These kinds of retrospective assessments of fibrotic staging will be valuable in estimating a long-term progression of liver disease, in evaluating efficacy of long-term medication or other medical intervention, or in making a political judgment from the viewpoints of socioeconomic efficacy.

The score can be calculated for any patients with chronic HBV infection. Although this multiple regression model dealt with appropriate logarithmic transformation for non-normal distribution parameters, the regression analysis was based on a linear regression model. Very slight fibrosis can be calculated as less than 1.00, which is commonly found to a slight degree in chronic hepatitis with tiny fibrotic change as F0. Very severe fibrosis might be calculated as more than 4.00, which is an imaginary and nonsense number in the scoring system of fibrosis. The FSB is, however, very useful and valuable in a real clinical setting: estimation of severity of liver fibrosis in an outpatient clinic, evaluation of the natural progression of a patient's fibrosis over 10 years and assessment of a long-term administration of interferon in patients with chronic hepatitis B from the viewpoint of fibrotic change. Recent development of new nucleoside/nucleotide analogs requires evaluation for long-term histological advantage, for aggravation of hepatitis stage during viral and biochemical breakthrough caused by HBV mutation, and even for

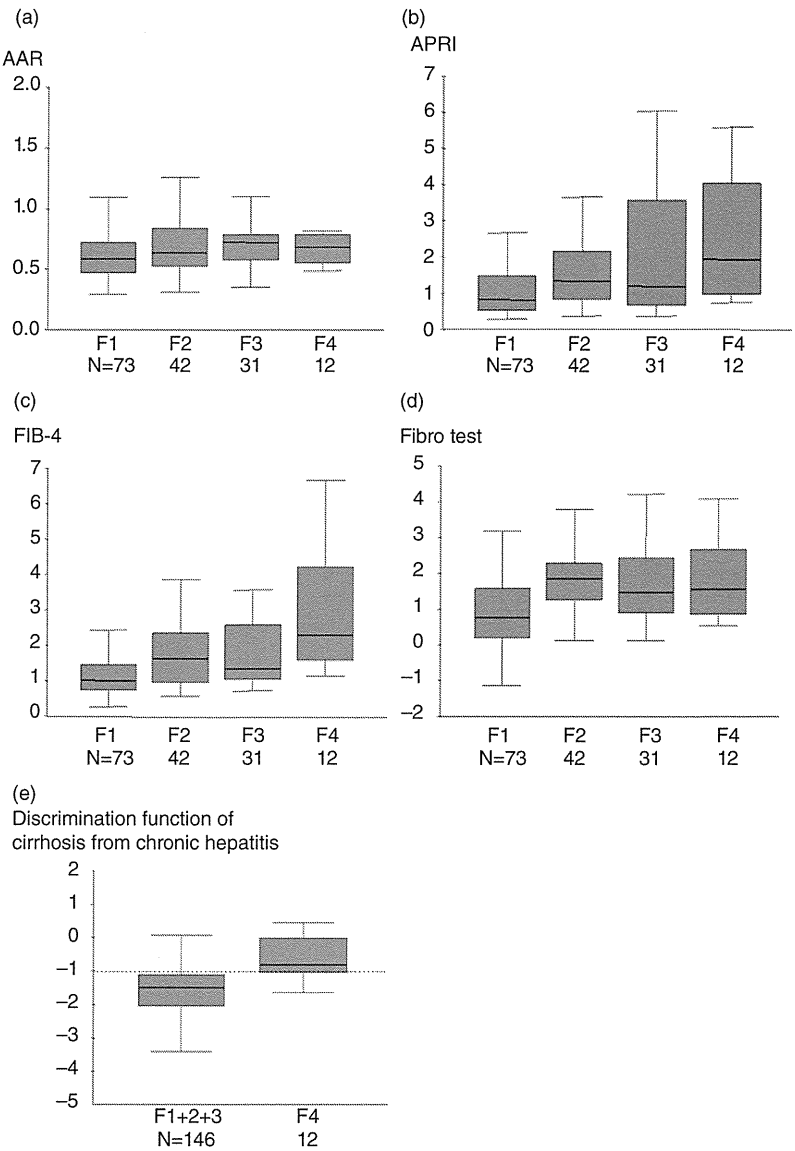

Figure 4 Previously published fibrosis scores. (a) Aspartate aminotransferase/alanine aminotransferase ratio (AAR),[19] (b) aspartate aminotransferase-to-platelet ratio index (APRI),[20] (c) FIB-4,[21] (d) FibroTest[22] and (e) discrimination function of cirrhosis from hepatitis in Japanese patients.[23]

the best management of patients with chronic hepatitis B. The FSB seems one of the ideal methods of approximating the fibrotic stage of chronic hepatitis B. Repeated measurement is quite suitable for patients with an unestablished treatment or trial, every 1 or 2 years, for example. Because the current regression function was generated from the data of HBV-related chronic liver disease, this equation would not be suitable for the recognition of hepatitis C virus-related chronic liver disease, alcoholic liver disease, and other congenital or autoimmune liver diseases. To recognize the latter diseases, other studies of individual diseases must be performed.

We compared the usefulness of the FSB with that of other fibrosis scores.[19–23] The more simple and less expensive AAR or APRI could not estimate fibrotic stages with poor correlation coefficients of 0.199 and 0.265, which are much lower than the coefficient of the FSB of 0.625. FibroTest, which contained three costly fibrosis markers (α-2-macroglobulin, haptoglobin and apolipo-

protein A1), also showed a low correlation coefficient of 0.330, suggesting that its usefulness was limited in HBV positive oriental patients. Although FIB-4 demonstrated the best coefficient of 0.412 among the fibrosis scores, significant overlaps were found between neighboring stages and obtained scores were not coordinated for real histological classification.

In conclusion, the FSB was a useful and reliable biomarker for prediction of liver fibrosis in patients with chronic HBV infection. The FSB is expected to be introduced and utilized in varied kinds of studies and trials. Its accuracy and reproducibility require further validation using higher numbers of patients in several countries other than Japan.

ACKNOWLEDGMENTS

THIS STUDY WAS proposed and initiated by Dr Shiro Iino and the project was performed with a grant from the Viral Hepatitis Research Foundation of Japan.

REFERENCES

1 Sandrin L, Fourquet B, Hasquenoph JM *et al.* Transient elastography: a new noninvasive method for assessment of hepatic fibrosis. *Ultrasound Med Biol* 2003; **29**: 1705–13.
2 Myers RP, Tainturier MH, Ratziu V *et al.* Prediction of liver histological lesions with biochemical markers in patients with chronic hepatitis B. *J Hepatol* 2003; **39**: 222–30.
3 Hanna RF, Kased N, Kwan SW *et al.* Double-contrast MRI for accurate staging of hepatocellular carcinoma in patients with cirrhosis. *AJR Am J Roentgenol* 2008; **190**: 47–57.
4 Hagiwara M, Rusinek H, Lee VS *et al.* Advanced liver fibrosis: diagnosis with 3D whole-liver perfusion MR imaging–initial experience. *Radiology* 2008; **246**: 926–34.
5 Taouli B, Chouli M, Martin AJ, Qayyum A, Coakley FV, Vilgrain V. Chronic hepatitis: role of diffusion-weighted imaging and diffusion tensor imaging for the diagnosis of liver fibrosis and inflammation. *J Magn Reson Imaging* 2008; **28**: 89–95.
6 Montazeri G, Estakhri A, Mohamadnejad M *et al.* Serum hyaluronate as a non-invasive marker of hepatic fibrosis and inflammation in HBeAg-negative chronic hepatitis B. *BMC Gastroenterol* 2005; **5**: 32.
7 Zeng MD, Lu LG, Mao YM *et al.* Prediction of significant fibrosis in HBeAg-positive patients with chronic hepatitis B by a noninvasive model. *Hepatology* 2005; **42**: 1437–45.
8 Chrysanthos NV, Papatheodoridis GV, Savvas S *et al.* Aspartate aminotransferase to platelet ratio index for fibrosis evaluation in chronic viral hepatitis. *Eur J Gastroenterol Hepatol* 2006; **18**: 389–96.
9 Kim BK, Kim Y, Park JY *et al.* Validation of FIB-4 and comparison with other simple noninvasive indices for predicting liver fibrosis and cirrhosis in hepatitis B virus-infected patients. *Liver Int* 2010; **30**: 546–53.
10 Wu SD, Wang JY, Li L. Staging of liver fibrosis in chronic hepatitis B patients with a composite predictive model: a comparative study. *World J Gastroenterol* 2010; **16**: 501–7.
11 Sökücü S, Gökçe S, Güllüoğlu M, Aydoğan A, Celtik C, Durmaz O. The role of the non-invasive serum marker FibroTest-ActiTest in the prediction of histological stage of fibrosis and activity in children with naïve chronic hepatitis B infection. *Scand J Infect Dis* 2010; **42**: 699–703.
12 Liu HB, Zhou JP, Zhang Y, Lv XH, Wang W. Prediction on liver fibrosis using different APRI thresholds when patient age is a categorical marker in patients with chronic hepatitis B. *Clin Chim Acta* 2011; **412**: 33–7.
13 Park SH, Kim CH, Kim DJ *et al.* Usefulness of Multiple Biomarkers for the Prediction of Significant Fibrosis in Chronic Hepatitis B. *J Clin Gastroenterol* 2011; **45**: 361–5.
14 Engstrom-Laurent A, Loof L, Nyberg A, Schroder T. Increased serum levels of hyaluronate in liver disease. *Hepatology* 1985; **5**: 638–42.
15 Murawaki Y, Ikuta Y, Koda M, Kawasaki H. Serum type III procollagen peptide, type IV collagen 7S domain, central triple-helix of type IV collagen and tissue inhibitor of metalloproteinases in patients with chronic viral liver disease: relationship to liver histology. *Hepatology* 1994; **20**: 780–7.
16 Fabris C, Falleti E, Federico E, Toniutto P, Pirisi M. A comparison of four serum markers of fibrosis in the diagnosis of cirrhosis. *Ann Clin Biochem* 1997; **34**: 151–5.
17 Desmet VJ, Gerber M, Hoofnagle JH, Manns M, Sheuer PJ. Classification of chronic hepatitis: diagnosis, grading, and staging. *Hepatology* 1994; **19**: 1513–20.
18 IBM SPSS Inc. *IBM SPSS for Windows Version 19.0 Manual.* Armonk NY, USA: SPSS Japan Inc., an IBM company, 2009.
19 Sheth SG, Flamm SL, Gordon FD *et al.* AST/ALT ratio predicts cirrhosis in patients with chronic hepatitis C virus infection. *Am J Gastroenterol* 1998; **93**: 44–8.
20 Wai CT, Greenson JK, Fontana RJ *et al.* A simple noninvasive index can predict both significant fibrosis and cirrhosis in patients with chronic hepatitis C. *Hepatology* 2003; **38**: 518–26.
21 Sterling RK, Lissen E, Clumeck N *et al.* Develoment of a simple noninvasive index to predict significant fibrosis in patients with HIV/HCV coinfection. *Hepatology* 2006; **43**: 1317–25.
22 Imbert-Bismut F, Ratziu V, Pieroni L *et al.* Biochemical imarkers of liver fibrosis in patients with hepatitis C virus infection: a prospective study. *Lancet* 2001; **357**: 1069–75.
23 Ikeda K, Saitoh S, Kobayashi M *et al.* Distinction between chronic hepatitis and liver cirrhosis in patients with hepatitis C virus infection. Practical Discriminant function using common laboratory data. *Hepatol Res* 2000; **18**: 252–66.
24 Lok ASF, McMahon BJ. AASLD Practice Guidelines. Chronic hepatitis B: update 2009. *Hepatology* 2009; **50**: 1–36.

J Gastroenterol (2013) 48:366–373
DOI 10.1007/s00535-012-0635-7

ORIGINAL ARTICLE—LIVER, PANCREAS, AND BILIARY TRACT

Perihepatic lymph node enlargement is a negative predictor of liver cancer development in chronic hepatitis C patients

Hiromi Hikita · Hayato Nakagawa · Ryosuke Tateishi · Ryota Masuzaki · Kenichiro Enooku · Haruhiko Yoshida · Masao Omata · Yoko Soroida · Mamiko Sato · Hiroaki Gotoh · Atsushi Suzuki · Tomomi Iwai · Hiromitsu Yokota · Kazuhiko Koike · Yutaka Yatomi · Hitoshi Ikeda

Received: 5 January 2012 / Accepted: 19 June 2012 / Published online: 12 July 2012

Abstract
Background Perihepatic lymph node enlargement (PLNE) is a common ultrasound finding in chronic hepatitis C patients. Although PLNE is considered to reflect the inflammatory response to hepatitis C virus (HCV), its clinical significance remains unclear.
Methods Between December 2004 and June 2005, we enrolled 846 chronic hepatitis C patients in whom adequate ultrasound examinations had been performed. PLNE was defined as a perihepatic lymph node that was at least 1 cm in the longest axis by ultrasonography. We analyzed the clinical features of patients with PLNE and prospectively investigated the association between PLNE and hepatocellular carcinoma (HCC) development.
Results We detected PLNE in 169 (20.0 %) patients. Female sex, lower body mass index (BMI), and HCV serotype 1 were independently associated with the presence of PLNE. However, there were no significant differences in liver function tests, liver stiffness, and hepatitis C viral loads between patients with and without PLNE. During the follow-up period (mean 4.8 years), HCC developed in 121 patients. Unexpectedly, patients with PLNE revealed a significantly lower risk of HCC development than those without PLNE ($p = 0.019$, log rank test). Multivariate analysis revealed that the presence of PLNE was an independent negative predictor of HCC development (hazard ratio 0.551, $p = 0.042$). In addition, the sustained viral response rate in patients who received interferon (IFN) therapy was significantly lower in patients with PLNE than in patients without PLNE.
Conclusions Patients with PLNE had a lower risk of HCC development than those without PLNE. This study may provide new insights into daily clinical practice and the pathophysiology of HCV-induced hepatitis and hepatocarcinogenesis.

Keywords Perihepatic lymph node enlargement · Chronic hepatitis C · Hepatocarcinogenesis

Abbreviations

ALT	Alanine aminotransferase
AFP	α-Fetoprotein
PLNE	Perihepatic lymph node enlargement
HCV	Hepatitis C virus
HCC	Hepatocellular carcinoma
IFN	Interferon
LN	Lymph node
US	Ultrasonography

Introduction

Hepatocellular carcinoma (HCC) is the fifth most common cancer worldwide and chronic hepatitis C virus (HCV)

H. Hikita and H. Nakagawa contributed equally to this work.

H. Hikita · H. Nakagawa · K. Enooku · Y. Soroida · M. Sato · H. Gotoh · A. Suzuki · T. Iwai · H. Yokota · Y. Yatomi · H. Ikeda
Department of Clinical Laboratory Medicine, Graduate School of Medicine, University of Tokyo, 7-3-1 Hongo, Bunkyo-ku, Tokyo 113-8655, Japan

H. Nakagawa (✉) · R. Tateishi · R. Masuzaki · K. Enooku · H. Yoshida · K. Koike · H. Ikeda
Department of Gastroenterology, Graduate School of Medicine, University of Tokyo, 7-3-1 Hongo, Bunkyo-ku, Tokyo 113-8655, Japan
e-mail: n-hayato@yf7.so-net.ne.jp

M. Omata
Yamanashi Prefectural Hospital Organization, 1-1-1 Fujimi, Kofu, Yamanashi 400-8506, Japan